I&EC research
Industrial & Engineering Chemistry Research

Article

Cite This: Ind. Eng. Chem. Res. 2019, 58, 12097−12115

pubs.acs.org/IECR

Economic Model-Based Controller Design Framework for Hydraulic Fracturing To Optimize Shale Gas Production and Water Usage

Kaiyu Cao,[†,‡] Prashanth Siddhamshetty,[†,‡] Yuchan Ahn,[†,‡] Rajib Mukherjee,[†,‡] and Joseph Sang-Il Kwon*[,†,‡]

[†]Texas A&M Energy Institute, Texas A&M University, College Station, Texas 77843, United States

[‡]Artie McFerrin Department of Chemical Engineering, Texas A&M University, College Station, Texas 77845, United States

Supporting Information

ABSTRACT: As water issues associated with hydraulic fracturing have received much attention, several optimization approaches have been developed for effective water management. However, most of them have not considered pumping schedules for hydraulic fracturing, which determine the productivity of a shale well as well as the total amount of freshwater required. Because of this, a novel model-based control framework is proposed for hydraulic fracturing to maximize the net profit from shale gas development which simultaneously minimizes the total cost associated with water management. The framework is as follows: initially a reduced-order model and a Kalman filter are developed based on the simulation data generated from a high-fidelity hydraulic fracturing model to correlate the pumping schedule and the final fracture geometry. Then, a numerical reservoir simulator and mixed-integer nonlinear programming model are used to generate two maps describing the revenue from selling shale gas produced and cost from managing wastewater recovered, respectively. Finally, by applying a data-based dynamic input−output model to connect the two maps, an economic model predictive control system is formulated. The proposed control framework enables 62% of the generated wastewater to be reused through the application of thermal membrane distillation technology in the treatment process and results in a 11% reduction in overall freshwater consumption, while maintaining the productivity of a shale well at its theoretical maximum.

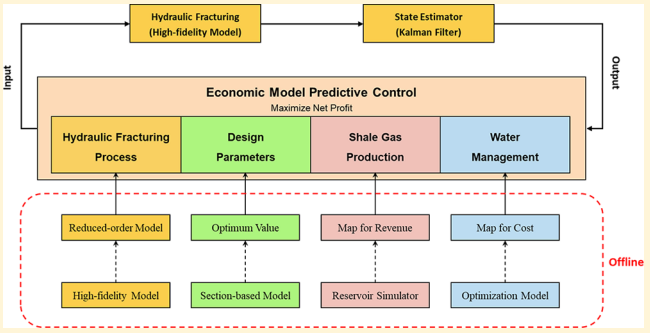

1. INTRODUCTION

Shale gas is an indispensable resource to satisfy the global energy demand, and it has resulted in an increase in the total energy production of the United States. As reported, the production from shale gas is the main contributor to the growth of natural gas production, being expected to account for nearly two-thirds of the total US production by 2040.[1] The exploration and development of shale gas will possibly allow the United States to become energy independent by 2026.[1] This rapid growth in shale gas production would not have happened without continued technological advancement and improvement. Since shale gas is characterized as an unconventional resource due to ultralow permeability of the rock formation, it has been extremely difficult and costly to extract the gas from shale rock in the past decades.[2] Recently, the combined use of horizontal drilling and hydraulic fracturing technologies has ramped up shale gas production and made it economically viable to develop unconventional reservoirs. The horizontal drilling makes it accessible to more targeted hydrocarbon zones from one surface location, which reduces the surface footprint of the drilling process. Even though the capital investment is increased comparing to vertical drilling, it is generally made up for with the improved efficiency of the exploitation process.[3] The hydraulic fracturing helps create high conductivity pathways for gas extraction and enhances formation permeability, which in turn increases the overall productivity of the fractured wells.

Despite the economic benefit of horizontal drilling and hydraulic fracturing technology, the concerns about the associated water issues have been growing. On average, about 3−6 million gallons of freshwater are used to complete a typical well.[4,5] Nearly 10% of this freshwater is used in the drilling process while the remaining 90% is required for the hydraulic fracturing operation, in which the injected water is mixed with proppant (most often sand) and chemical additives to make up the fracturing fluid for the propagation of fractures.[6] Since many sites can contain several well pads which allow multiple horizontal wells to be drilled and fracking process takes only 2−3 days, a serious problem is that a considerable amount of freshwater must be supplied within a relatively short time.[7] Another issue that appears in the post-fracturing process is water contamination. After hydraulic fracturing, a certain amount of the injected fracturing fluid flows back to the surface as wastewater, containing high concentrations of various con-

Received: March 21, 2019
Revised: May 9, 2019
Accepted: June 17, 2019
Published: June 17, 2019

DOI: 10.1021/acs.iecr.9b01553
Ind. Eng. Chem. Res. 2019, 58, 12097−12115

taminants such as the total dissolved solids (TDS), metals, total suspended solids (TSS), naturally occurring radioactive material (NORM), organics, and hydrocarbons.[6,8] Since the conventional disposal option of deep well injection is not necessarily available near the drilling sites and fracturing fluid becomes more tolerant of contaminants, the demand for treatment of wastewater for recycle and reuse has been recently increased.[9] In general, the quality of wastewater generated from hydraulic fracturing can be determined by the amount of TDS per liter of water.[10,11] Removal of the TDS can be achieved using several available treatment technologies including reverse osmosis (RO), membrane distillation (MD), evaporation, and crystallization.[9,12−17] However, selection of the proper technology depends on the TDS concentration in the wastewater, required purification level for recycle and reuse, operating condition in the hydraulic fracturing process, and capacity of the treatment technology. Since the characteristics of shale formation vary from region to region, the recovery ratio, TDS concentration, and flow rate of the generated wastewater can be significantly different. In addition, the differences in state regulatory policies and economic factors may also affect the strategy for effective water management. Thus, with the difficulty in supplying sufficient freshwater to drilling sites and the instability of wastewater treatment, developing an environmentally sustainable and economically viable water management plan along with optimizing production is crucial.

In this regard, several strategies to effectively manage water in shale gas development have been developed using optimization techniques.[5,8−10,18,19] Yang et al. developed a two-stage stochastic mixed-integer linear programming (MILP) model for operational scheduling problem while minimizing the freshwater consumption and the total cost in the water cycle.[8] To consider the decisions on strategic design, they extended the previous work and presented a comprehensive MILP model for capital investment decisions as well as the scheduling for long-term operation.[9] Gao and You proposed a novel mixed-integer linear fractional programming (MILFP) model and associated global optimization algorithm for optimal design of water supply networks.[10] Lira-Barragan et al. expanded the commonly used optimization framework to include the uncertainties related to the amount of injected freshwater and generated wastewater.[5] Lopez Diaz et al. developed a multi-objective optimization model for water networks, which presents the trade-offs between the economic and environmental objectives by minimizing the total annual cost (TAC) and maximizing the removal of pollutants.[19] Oke et al. developed a mixed-integer nonlinear programming (MINLP) model by applying continuous time scheduling formulations and detailed membrane distillation models, which simultaneously optimizes the water and energy consumption in the integrated water and membrane distillation network.[18] However, these studies did not consider hydraulic fracturing as a dynamic process, in which the flow rate of fracturing fluid, some of which contains freshwater, should be determined by a controller to maximize productivity of the fractured wells. In the hydraulic fracturing operation, the pumping schedule, including the flow rate and the proppant concentration of the injecting fracturing fluid, is critical. It determines the volume of freshwater needed for blending and directly affects the proppant distribution inside the created fractures, which influences the fracture conductivity and thus the production rate of shale gas. Over the last few decades, several efforts have been made to obtain the optimal pumping schedule while achieving the uniform proppant concentration and the prescribed fracture geometry at the end of pumping.[20−28] Specifically, Siddhamshetty et al. developed a model-based feedback control system which can compute the optimal pumping schedule to achieve a uniform proppant bank height over the optimal fracture length at the end of pumping.[23] However, this pumping schedule was obtained neglecting the environmental and the economic impacts of the water management.

Recently, Etoughe et al. proposed a new framework integrating the optimization work of water management into the model-based pumping schedule design of hydraulic fracturing, which minimizes the freshwater consumption as well as the total annual cost from water management and reduces the negative environmental impact.[29] In their work, the feedback control system developed by Siddhamshetty et al. was used to determine the optimal pumping schedule with a reduced amount of freshwater, which maximizes the productivity of the fractured well.[23] Then, a MINLP model was developed to determine the corresponding optimal water management strategy and mitigate the environmental toxicity by treating the flowback water through membrane distillation technology. Although this study provided an idea that the required freshwater consumption can be reduced by manipulating the pumping schedule, the resultant optimal water management could have negative impacts on the productivity, which was not considered because of the open-loop nature of the developed framework. That is, injecting less water, which is not sufficient to achieve the optimal fracture geometry at the end of pumping, may be beneficial from the water management perspective, while the final fracture geometry may result in a decrease in productivity. On the contrary, if the optimal fracture geometry is desired, which requires more freshwater in hydraulic fracturing operation, there will be an increase in the total cost from water management. Thus, these two processes are negatively correlated and it is imperative to develop a closed-loop framework accounting for the trade-off between the water management cost and the shale gas production.

Motivated by these considerations, the focus of this study is to propose a novel controller design framework for hydraulic fracturing while considering the impact of water management. To establish the closed-loop control system, a mapping-based technique is proposed. In the modeling of wastewater management, a dynamic input−output model is developed based on field data to establish the correlation between pumping schedule (i.e., volume of injected freshwater) and characteristics of recovered wastewater (i.e., flow rate and TDS concentration). Then, a MINLP optimization model is developed with the incorporation of a thermal membrane distillation (TMD) model. After solving the optimization problem with multiple operating conditions (i.e., different flow rate and TDS concentration profiles of generated wastewater), one map representing the relationship between the total wastewater management cost and the total volume of injected freshwater is obtained offline. In the modeling of hydraulic fractures, the reservoir simulation software from Computer Modeling Group Ltd. (CMG) is used to generate the shale gas production profile based on propped fracture geometry. By running CMG with multiple fracture geometries and taking into account the selling price of shale gas, another map representing the relationship between the total revenue from shale gas production and the propped fracture geometry is also obtained offline. Then, a section-based optimization method is used to determine the key design parameters required in this simulation. Finally, applying

DOI: 10.1021/acs.iecr.9b01553
Ind. Eng. Chem. Res. 2019, 58, 12097−12115

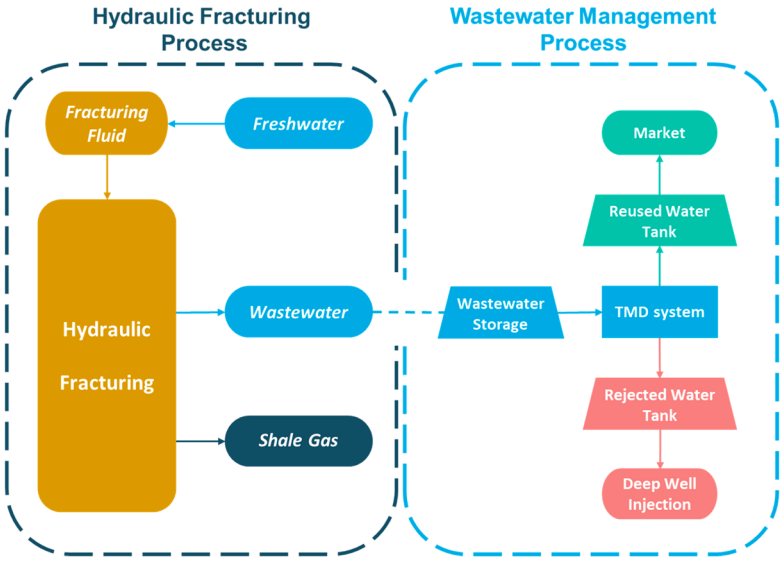

Figure 1. Schematic flow diagram for shale gas development.

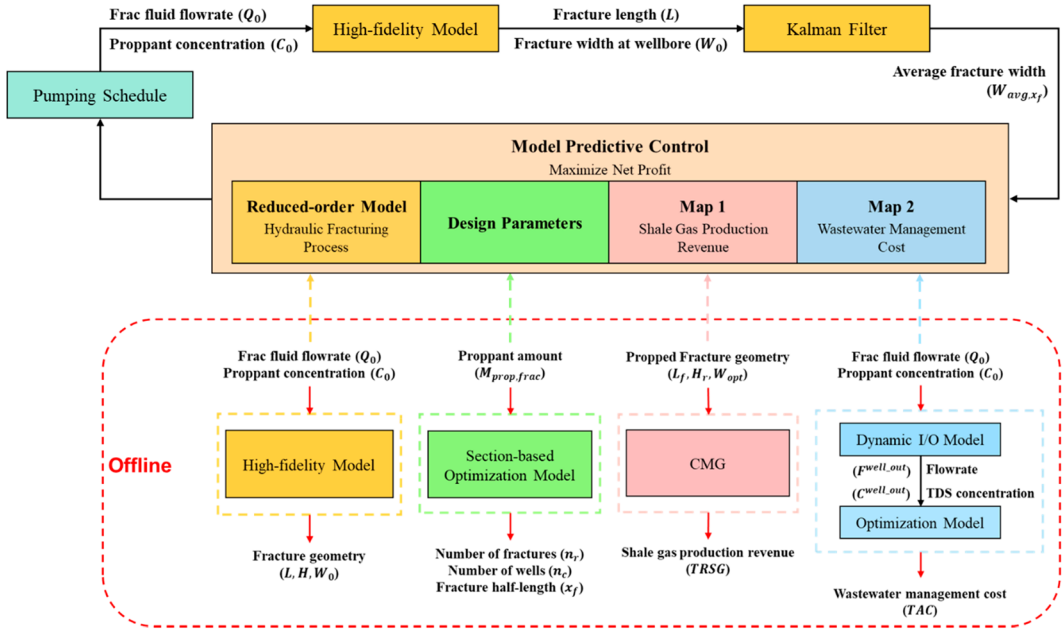

Figure 2. Schematic diagram for shale gas development.

the two maps to the feedback control system for hydraulic fracturing and considering the purchase of freshwater to make up the fracturing fluid, a new model predictive control (MPC) formulation is developed to determine the optimal pumping schedule which maximizes the net profit from shale gas development by simultaneously considering the revenue from shale gas production and the cost from water management (i.e., cost from purchasing freshwater and managing wastewater).

This paper is organized as follows. Section 2 presents the developed diagrams of the integrated control framework. The detailed information about the proposed mathematical model for the wastewater management and the formulations for the MPC system are presented in section 3. In section 4, the results and discussion are described. Finally, several conclusions are given in section 5.

2. METHODOLOGY

Figure 1 shows a schematic flow diagram constructed to represent the shale gas development, which can be divided into two subsections. Figure 2 represents the algorithmic diagram of the proposed control framework.

As shown in Figure 2, since the objective of this closed-loop MPC system is to maximize the net profit from shale gas development, the models for hydraulic fracturing process, shale gas production, and wastewater management are considered in this work. Specifically, the cost of purchasing the freshwater is also included in this MPC system and can be easily calculated based on the pumping schedule (i.e., flow rate and proppant concentration of injected fracturing fluid).

In modeling the hydraulic fracturing process, a high-fidelity hydraulic fracturing model developed by Siddhamshetty et al.[23]

DOI: 10.1021/acs.iecr.9b01553
Ind. Eng. Chem. Res. 2019, 58, 12097−12115

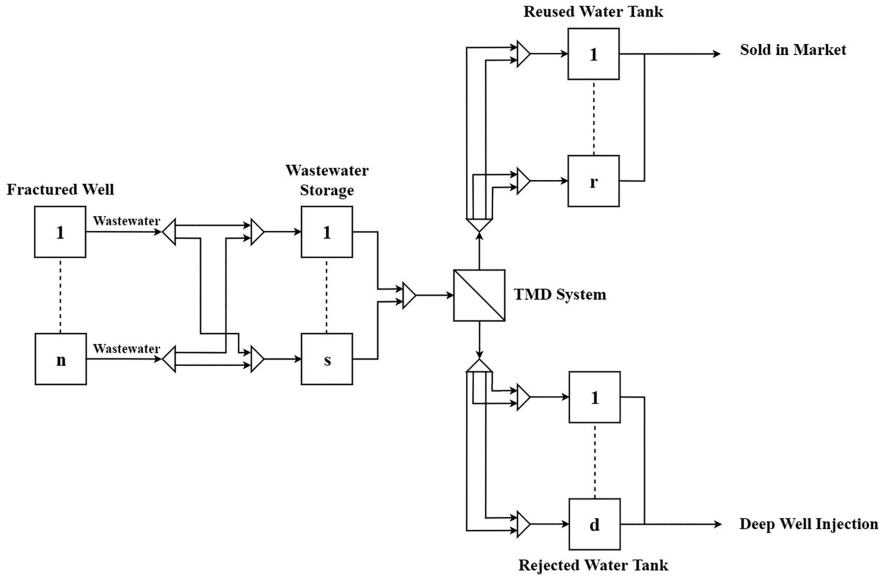

Figure 3. Schematic flow diagram for the optimization model of wastewater management.

is considered so that the final fracture geometry at the end of pumping (i.e., fracture length, fracture width and fracture height) and the pumping schedule are correlated. Using CMG software and considering the selling price of shale gas, the gas production profile and the corresponding revenue can be obtained. Then, in the modeling of wastewater management, the TMD technology is applied for the wastewater treatment process and thus a mathematical model based on the integrated water and TMD network shown in Figure 1 is developed to minimize the cost associated with the wastewater management. Since it is presented in Figure 1 that the connection between the hydraulic fracturing process and the wastewater management process is the "wastewater", a dynamic input−output model is developed in this work to generate the flow rate and TDS concentration of wastewater based on the pumping schedule (i.e., volume of injected freshwater), which are used as the inputs to the developed optimization model.

To formulate MPC system and reduce the computational requirement, the reduced-order model (ROM) and a mapping-based technique are applied in this work. Based on the input/output simulation data generated by the high-fidelity process model, CMG software and wastewater management optimization model, the ROM representing the hydraulic fracturing process, one map representing the shale gas production revenue and another map representing the wastewater management cost are developed. Thus, along with the section-based optimization model used to determine key design parameters required (i.e., number of wells, number of fractures and fracture half-length), the MPC system is formulated. It is noted that the Kalman filter is developed based on the developed ROM and the measurements (i.e., fracture length and fracture width at the wellbore) to estimate the unmeasurable variable (i.e., fracture average width), which determines the propped fracture geometry (i.e., propped fracture length and propped fracture width) and is implemented as an important constraint in this control framework.

3. MODEL FORMULATION

3.1. Optimization Modeling for Wastewater Management. In this section, the superstructure for the wastewater management is developed, as shown in Figure 3.

A set of (N) fractured wells, (S) storage units, (R) reuse units, (D) disposal units, and one $(A = 1)$ treatment unit are included in this network, and the problem is addressed over a time horizon which is divided into (T) identical time intervals. The subscripts n, s, r, d, a, and t are used to represent the fractured wells, wastewater storages, reused water tanks in reuse units, rejected water tanks in disposal units, TMD system, and time periods, respectively. Note that in the reuse units, the temporarily stored reused water is then sold in the market for drinking, urban, or agricultural purposes. In the disposal units, the temporarily stored rejected water is then injected down the well and deep into the earth. More details about the TMD system are discussed in section 3.1.2.

As Figure 3 shows, the wastewater coming out from the fractured wells can be stored in the storage near the drilling sites, and will be transported to the TMD system to remove the TDS. All the collected wastewater is treated before being reused, or being directly dumped in disposal wells. Note that in this study, it is assumed that the reused water is sold in the market instead of being reintroduced as part of the fracturing fluid for drilling other shale wells. On the basis of the developed superstructure in Figure 3, a MINLP optimization model is presented for the optimal design and operation for wastewater management in the post-fracturing process, which is divided into three subsections. The first subsection focuses on the mass and contaminant balances and constraints; the second presents a detailed TMD model; the third gives all the associated costs and the overall objective function.

3.1.1. Balance and Constraint. Mass and Contaminant Balance around Fractured Wells. The wastewater recovered from hydraulic fracturing is transported to the wastewater storages. Equation 1 states that the wastewater generated from fractured well n in time period t ($F_{n,t}^{\text{well\_out}}$) is segregated and sent to each wastewater storage s during the same time period ($ff_{n,s,t}^{\text{well\_storage}}$). Equation 2 presents the corresponding TDS mass flow of the stream ($mm_{n,s,t}^{\text{well\_storage}}$) that comes out of well n into storage s in time period t, based on the segregated flow rate ($ff_{n,s,t}^{\text{well\_storage}}$) and TDS concentration ($C_{n,t}^{\text{well\_out}}$) of the wastewater leaving well n in time period t.

DOI: 10.1021/acs.iecr.9b01553
Ind. Eng. Chem. Res. 2019, 58, 12097−12115

$$F_{n,t}^{\text{well\_out}} = \sum_{s} ff_{n,s,t}^{\text{well\_storage}}, \quad \forall\, n, \forall\, t \tag{1}$$

$$mm_{n,s,t}^{\text{well\_storage}} = C_{n,t}^{\text{well\_out}} ff_{n,s,t}^{\text{well\_storage}}, \quad \forall\, n, \forall\, s, \forall\, t \tag{2}$$

Mass and Contaminant Balance around Storage Units. The outlet streams from different wells are blended in the inlet of storage s. Equations 3 and 4 describe the segregation of flow rate ($F_{s,t}^{\text{storage\_in}}$) and TDS mass flow rate ($M_{s,t}^{\text{storage\_in}}$) of the mixture fluid entering storage s in time period t, respectively.

$$F_{s,t}^{\text{storage\_in}} = \sum_{n} ff_{n,s,t}^{\text{well\_storage}}, \quad \forall\, s, \forall\, t \tag{3}$$

$$M_{s,t}^{\text{storage\_in}} = \sum_{n} mm_{n,s,t}^{\text{well\_storage}}, \quad \forall\, s, \forall\, t \tag{4}$$

The TDS concentration of the mixture fluid ($C_{s,t}^{\text{storage\_in}}$) entering storage s in time point t is calculated in eq 5.

$$C_{s,t}^{\text{storage\_in}} = \frac{M_{s,t}^{\text{storage\_in}}}{F_{s,t}^{\text{storage\_in}}}, \quad \forall\, s, \forall\, t \tag{5}$$

Considering the tank as a continuous model, the mass balance equations for storage s in time period t are constructed in terms of the volume of stored wastewater ($V_{s,t}^{\text{storage}}$), as stated in eqs 6−8. They represent that the volume change of the stored wastewater from time period $t-1$ is the difference between the amount of wastewater entering and leaving the storage in time period t as follows:

$$V_{s,t}^{\text{storage}} = V_{s}^{\text{storage\_initial}} + H^{\text{time}}(F_{s,t}^{\text{storage\_in}} - F_{s,t}^{\text{storage\_out}}), \quad \forall\, s, \forall\, t = 1 \tag{6}$$

$$V_{s,t}^{\text{storage}} = V_{s,t-1}^{\text{storage}} + H^{\text{time}}(F_{s,t}^{\text{storage\_in}} - F_{s,t}^{\text{storage\_out}}), \quad \forall\, s, \forall\, t > 1 \tag{7}$$

$$V_{s,t}^{\text{storage}} = 0, \quad \forall\, s, \forall\, t = \text{end} \tag{8}$$

Similarly, the contaminant balance equations in terms of the TDS concentration are constructed as shown in eqs 9−11.

$$C_{s,t}^{\text{storage\_out}} = C_{s,t}^{\text{storage\_in}}, \quad \forall\, s, \forall\, t = 1 \tag{9}$$

$$C_{s,t}^{\text{storage\_out}} V_{s,t}^{\text{storage}} = C_{s,t-1}^{\text{storage\_out}} V_{s,t-1}^{\text{storage}} + H^{\text{time}} C_{s,t}^{\text{storage\_in}} F_{s,t}^{\text{storage\_in}} - H^{\text{time}} C_{s,t}^{\text{storage\_out}} F_{s,t}^{\text{storage\_out}}, \quad \forall\, s, \forall\, t > 1 \tag{10}$$

$$0 = C_{s,t-1}^{\text{storage\_out}} V_{s,t-1}^{\text{storage}} + H^{\text{time}} C_{s,t}^{\text{storage\_in}} F_{s,t}^{\text{storage\_in}} - H^{\text{time}} C_{s,t}^{\text{storage\_out}} F_{s,t}^{\text{storage\_out}}, \quad \forall\, s, \forall\, t = end \tag{11}$$

where $V_{s}^{\text{storage\_initial}}$ is the initial wastewater volume in storage s and H^{time} is the operation time in each time period. Specifically, eq 8 implies that there should be no wastewater stored in any tanks at the end of wastewater management process (t = end). $F_{s,t}^{\text{storage\_out}}$ and $C_{s,t}^{\text{storage\_out}}$ are the continuous variables specifying the flow rate and the TDS concentration of the wastewater stream leaving storage s in time period t. This wastewater stream is separated and sent to the TMD system, as stated in eq 12. With the TDS concentration of the outlet stream ($C_{s,t}^{\text{storage\_out}}$) from storage s in time period t, the corresponding mass flow rate of TDS ($mm_{s,a,t}^{\text{storage\_treatment}}$) is presented in eq 13.

$$F_{s,t}^{\text{storage\_out}} = \sum_{a} ff_{s,a,t}^{\text{storage\_treatment}}, \quad \forall\, s, \forall\, t \tag{12}$$

$$mm_{s,a,t}^{\text{storage\_treatment}} = C_{s,t}^{\text{storage\_out}} ff_{s,a,t}^{\text{storage\_treatment}}, \quad \forall\, s, \forall\, a, \forall\, t \tag{13}$$

Mass and Contaminant Balance around Treatment Unit. The wastewater entering the TMD system is supplied by the outlet streams from storages, as stated in eq 14. Equations 15 and 16 indicate the total mass flow rate of TDS ($M_{a,t}^{\text{treatment\_in}}$) and the calculated TDS concentration ($C_{a,t}^{\text{treatment\_in}}$) respectively in the inlet stream to the TMD system a in time period t.

$$F_{a,t}^{\text{treatment\_in}} = \sum_{s} ff_{s,a,t}^{\text{storage\_treatment}}, \quad \forall\, a, \forall\, t \tag{14}$$

$$M_{a,t}^{\text{treatment\_in}} = \sum_{s} mm_{s,a,t}^{\text{storage\_treatment}}, \quad \forall\, a, \forall\, t \tag{15}$$

$$C_{a,t}^{\text{treatment\_in}} = \frac{M_{a,t}^{\text{treatment\_in}}}{F_{a,t}^{\text{treatment\_in}}}, \quad \forall\, a, \forall\, t \tag{16}$$

After the treatment process, the treated water can be sent to the reuse or disposal units. Equation 17 states that the flow rate of wastewater to be treated entering TMD system a in time period t ($F_{a,t}^{\text{treatment\_in}}$) is the sum of the flow rate of the permeate streams that will be sent to reused water tanks ($ff_{a,r,t}^{\text{treatment\_reuse}}$) and the flow rate of the concentrate streams that will be sent to rejected water tanks ($ff_{a,r,t}^{\text{treatment\_disposal}}$). Similarly, eqs 18−20 describe the mass flow rate of TDS and the TDS concentration in the outlet streams of the TMD system a.

$$F_{a,t}^{\text{treatment\_in}} = \sum_{r} ff_{a,r,t}^{\text{treatment\_reuse}} + \sum_{d} ff_{a,d,t}^{\text{treatment\_disposal}}, \quad \forall\, a, \forall\, t \tag{17}$$

$$M_{a,t}^{\text{treatment\_in}} = \sum_{r} mm_{a,r,t}^{\text{treatment\_reuse}} + \sum_{d} mm_{a,d,t}^{\text{treatment\_disposal}}, \quad \forall\, a, \forall\, t \tag{18}$$

$$C_{a,r,t}^{\text{treatment\_reuse}} = \frac{mm_{a,r,t}^{\text{treatment\_reuse}}}{ff_{a,r,t}^{\text{treatment\_reuse}}}, \quad \forall\, a, \forall\, r, \forall\, t \tag{19}$$

$$C_{a,d,t}^{\text{treatment\_disposal}} = \frac{mm_{a,d,t}^{\text{treatment\_disposal}}}{ff_{a,d,t}^{\text{treatment\_disposal}}}, \quad \forall\, a, \forall\, d, \forall\, t \tag{20}$$

Mass and Contaminant Balance around Reuse and Disposal Units. The flow rate of the reused water entering reused water tank r in time point t ($V_{r,t}^{\text{reuse\_in}}$) is supplied by the permeate streams of the TMD system ($ff_{a,r,t}^{\text{treatment\_reuse}}$) while the flow rate of the rejected water entering rejected water tank d in time period t ($F_{d,t}^{\text{disposal\_in}}$) is supplied by the concentrate streams of the TMD system ($ff_{a,d,t}^{\text{treatment\_disposal}}$). Assuming that the stream entering reused water tank r in time period t should be sold out at the end of the same time period, the amount of the water temporarily stored in the reused water tank r in time period t ($V_{r,t}^{\text{reuse}}$) can be presented as stated in eq 23. Equation 24 represents the same situation for the disposal units.

DOI: 10.1021/acs.iecr.9b01553
Ind. Eng. Chem. Res. 2019, 58, 12097−12115

$$F_{r,t}^{\text{reuse\_in}} = \sum_{a} ff_{a,r,t}^{\text{treatment\_reuse}}, \quad \forall\, r, \forall\, t \tag{21}$$

$$F_{d,t}^{\text{disposal\_in}} = \sum_{a} ff_{a,d,t}^{\text{treatment\_disposal}}, \quad \forall\, d, \forall\, t \tag{22}$$

$$V_{r,t}^{\text{reuse}} = H^{\text{time}} F_{r,t}^{\text{reuse\_in}}, \quad \forall\, r, \forall\, t \tag{23}$$

$$V_{d,t}^{\text{disposal}} = H^{\text{time}} F_{d,t}^{\text{disposal\_in}}, \quad \forall\, d, \forall\, t \tag{24}$$

Design Constraint for Storage, Reuse, and Disposal Units. The optimal design is achieved by determining the optimum number as well as the optimum size of each unit. Except for the TMD system, the constraints on the other units are formulated based on given maximum capacity. Binary variables are added to determine the number of established units. Equations 25 and 26 state that the capacity of storage s should not exceed the maximum capacity, and the corresponding binary variable indicates if this storage is required. Similarly, eqs 27 and 28 describe the constraints on the reuse units, and eqs 29 and 30 describe the constraints on the disposal units.

$$V_{s,t}^{\text{storage}} \le V_{s}^{\text{storage\_capacity}}, \quad \forall\, s, \forall\, t \tag{25}$$

$$V_{s}^{\text{storage\_capacity}} \le V_{s}^{\text{storage\_max}} y_{s}^{\text{storage}}, \quad \forall\, s \tag{26}$$

$$V_{r,t}^{\text{reuse}} \le V_{r}^{\text{reuse\_capacity}}, \quad \forall\, r, \forall\, t \tag{27}$$

$$V_{r}^{\text{reuse\_capacity}} \le V_{r}^{\text{reuse\_max}} y_{r}^{\text{reuse}}, \quad \forall\, r \tag{28}$$

$$V_{d,t}^{\text{disposal}} \le V_{d}^{\text{disposal\_capacity}}, \quad \forall\, d, \forall\, t \tag{29}$$

$$V_{d}^{\text{disposal\_capacity}} \le V_{d}^{\text{disposal\_max}} y_{d}^{\text{disposal}}, \quad \forall\, d \tag{30}$$

3.1.2. Thermal Membrane Distillation (TMD) Model. The detailed design model for TMD system is based on the work of Elsayed et al.[30] A typical TMD module is presented in Figure 4.

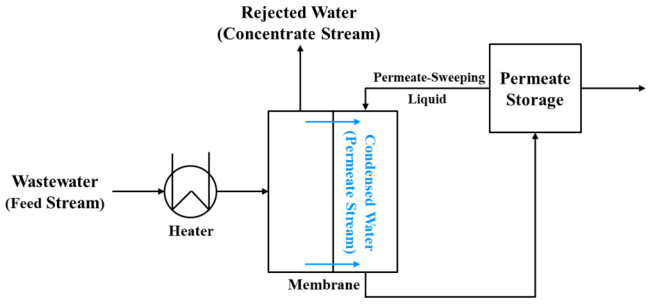

Figure 4. Schematic diagram for the TMD system.

In the TMD system, the wastewater in the inlet is preheated to achieve the vapor−liquid equilibrium and thus remove organics and the other contaminants. The water vapor passes through the membrane and is condensed as a highly pure liquid on the permeate side. The driving force for water flux ($J_{a,t}$) across the membrane in the TMD system a in time period t is the difference in chemical potential which is dependent on the vapor pressure difference between the feed and the permeate sides as stated in eq 31.

$$J_{a,t} = B_w(P_{\text{feed}}^{v}\gamma_{w,\text{feed},a,t}x_{w,\text{feed},a,t} - P_{\text{perm}}^{v}), \quad \forall\, a, \forall\, t \tag{31}$$

where $\gamma_{w,\text{feed},a,t}$ and $x_{w,\text{feed},a,t}$ are the activity coefficient and the mole fraction of the wastewater entering the TMD system a in time period t, B_w is the membrane permeability, P_{feed}^{v} is the water vapor pressure of feed stream and P_{perm}^{v} is the water vapor pressure of the permeate stream. Equations 32 and 33 describe the water vapor pressures via the Antoine equation, and eq 34 is proposed to determine the membrane permeability (B_w) of the TMD system.[31]

$$P_{\text{feed}}^{v} = \exp\left(23.1964 - \frac{3816.44}{T_{m,\text{feed}} - 46.13}\right) \tag{32}$$

$$P_{\text{perm}}^{v} = \exp\left(23.1964 - \frac{3816.44}{T_{m,\text{perm}} - 46.13}\right) \tag{33}$$

$$B_w = B_{wb}T_m^{1.334} \tag{34}$$

$$T_m = \frac{T_{b,\text{feed}} + T_{b,\text{perm}}}{2} = \frac{T_{m,\text{feed}} + T_{m,\text{perm}}}{2} \tag{35}$$

where $T_{m,\text{feed}}$ and $T_{m,\text{perm}}$ are the temperatures of the feed stream and the permeate stream on the membrane, while $T_{b,\text{feed}}$ and $T_{b,\text{perm}}$ are the bulk temperatures of the feed stream and the permeate stream, B_{wb} is the temperature-independent base value for permeability which is determined based on experimental data. Thus, the average membrane temperature T_m is defined in eq 35. Since the differences between $T_{m,\text{feed}}$ and $T_{b,\text{feed}}$, and $T_{m,\text{perm}}$ and $T_{b,\text{perm}}$ are almost the same, T_m can be calculated using the membrane temperature.[30] In this study, we assume that the feed stream is preheated to 363 K and the temperature difference is kept constant as 25 K, thus P_{feed}^{v}, P_{perm}^{v} and B_w are fixed parameters.

Assuming the primary solute in the wastewater is NaCl, with the TDS concentration of the stream entering the TMD system a in time period t ($C_{a,t}^{\text{treatment\_in}}$), the molar concentration of water ($x_{w,\text{feed},a,t}$) and the activity coefficient of water ($\gamma_{w,\text{feed},a,t}$) entering the TMD system a in time period t are calculated using eqs 36−38.[32]

$$x_{\text{NaCl,feed},a,t} = \frac{\frac{C_{a,t}^{\text{treatment\_in}}}{58}}{\frac{C_{a,t}^{\text{treatment\_in}}}{58} + \frac{1 - C_{a,t}^{\text{treatment\_in}}}{18}}, \quad \forall\, a, \forall\, t \tag{36}$$

$$x_{w,\text{feed},a,t} = 1 - x_{NaCl,\text{feed},a,t}, \quad \forall\, a, \forall\, t \tag{37}$$

$$\gamma_{w,\text{feed},a,t} = 1 - 0.5x_{\text{NaCl,feed},a,t} - 10x_{\text{NaCl,feed},a,t}^{2}, \quad \forall\, a, \forall\, t \tag{38}$$

Thus, the decision variable, which is the area of the membrane ($A_{m,a}$) required for the TMD system a, is determined using eqs 39 and 40. Then, the corresponding annual operation cost ($Cost_{a,t}^{\text{treatment}}$) and the annual capital cost ($CapCost_{a,t}^{\text{treatment}}$) for the TMD system a in time period t are given as eqs 41 and 42.[30] The water recovery ($\zeta_{a,t}$), which is defined as the flow rate ratio of the permeate stream to the feed stream, and the recycle ratio ($\upsilon_{a,t}$), which is defined as the flow rate ratio of the concentrate stream to the feed stream, are calculated using eqs 43 and 44. Note that the associated costs of the TMD system are dependent on $A_{m,a}$ and $F_{a,t}^{\text{treatment\_in}}$. Since there are no specific constraints on these key variables, it is assumed that there is only one TMD system in this network, which is capable of dealing with all the generated wastewater.

DOI: 10.1021/acs.iecr.9b01553
Ind. Eng. Chem. Res. 2019, 58, 12097−12115

$$A_{m,a,t} = \frac{\sum_r ff_{a,r,t}^{\text{treatment\_reuse}}}{J_{a,t}}, \quad \forall\, a, \forall\, t \tag{39}$$

$$A_{m,a} \geq A_{m,a,t}, \quad \forall\, a, \forall\, t \tag{40}$$

$$Cost_{a,t}^{\text{treatment}} = [1411 + 43(1 - \zeta_{a,t}) + 1613(1 + \upsilon_{a,t})]F_{a,t}^{\text{treatment\_in}}, \quad \forall\, a, \forall\, t \tag{41}$$

$$CapCost_{a,t}^{\text{treatment}} = 58.5A_{m,a} + 1115F_{a,t}^{\text{treatment\_in}}, \quad \forall\, a, \forall\, t \tag{42}$$

$$\zeta_{a,t} = \frac{\sum_r ff_{a,r,t}^{\text{treatment\_reuse}}}{F_{a,t}^{\text{treatment\_in}}}, \quad \forall\, a, \forall\, t \tag{43}$$

$$\upsilon_{a,t} = \frac{\sum_d ff_{a,d,t}^{\text{treatment\_disposal}}}{F_{a,t}^{\text{treatment\_in}}}, \quad \forall\, a, \forall\, t \tag{44}$$

As mentioned, the permeate streams are highly pure liquid, thus complete rejection is assumed. To avoid the buildup of contaminants and precipitation in the TMD system, the TDS weight fraction in the concentrate streams should not exceed 0.35. The constraints on the TDS weight fraction are presented in eqs 45 and 46.[30]

$$C_{a,r,t}^{\text{treatment\_reuse}} = 0, \quad \forall\, a, \forall\, r, \forall\, t \tag{45}$$

$$C_{a,d,t}^{\text{treatment\_disposal}} \leq 0.35, \quad \forall\, a, \forall\, d, \forall\, t \tag{46}$$

where if $C_{a,d,t}^{\text{treatment\_disposal}} = 0.35$, $\zeta_{a,t}$ should reach its maximum value. Hence, an implicit constraint is described in eq 47.[30]

$$\zeta_{a,t} \leq 1 - \frac{C_{a,t}^{\text{treatment\_in}}}{0.35}, \quad \forall\, a, \forall\, t \tag{47}$$

REMARK 1. The dynamics of the membrane separation processes may become significant if there is the fouling effect of the membrane.[33] For example, in reverse osmosis (RO), the permeability may change dynamically due to the fouling effect, as a result of the low rejection rate. However, TMD has a high rejection factor, which is validated through the principle of vapor−liquid equilibrium, and its membrane pore size is relatively larger than other membrane separation processes, such as RO. Therefore, TMD has very low fouling and it is not necessary to consider the membrane's dynamics in this work.[32]

3.1.3. Objective Function. The objective of the developed MINLP optimization model is to minimize the TAC, accounting for the operation cost (associated with transportation, TMD system, and disposal units), the capital cost (associated with storage units, TMD system, reuse units, and disposal units), and the revenue (associated with reuse units).

Treatment Cost. As discussed in section 3.1.2, the total operating cost for the TMD system is stated in eq 48. Note that $|t|$ is the number of the time periods considered

$$Cost^{\text{treatment}} = \frac{\sum_{a,t}[1411 + 43(1 - \zeta_{a,t}) + 1613(1 + \upsilon_{a,t})]F_{a,t}^{\text{treatment\_in}}}{|t|} \tag{48}$$

Disposal Cost. Given the unit operating cost for a disposal unit (UOC^{disposal}), the total disposal cost is presented in eq 49.

$$Cost^{\text{disposal}} = \sum_{d,t} UOC^{\text{disposal}} F_{d,t}^{\text{disposal\_in}} \tag{49}$$

Transportation Cost. Given the unit transportation costs (UTC) between units, the associated transportation costs are stated in eqs 50−53 and the total transportation cost is obtained as eq 54.

$$TransCost^{\text{well\_storage}} = H^{\text{time}} \sum_{n,s,t} UTC^{\text{well\_storage}} ff_{n,s,t}^{\text{well\_storage}} \tag{50}$$

$$TransCost^{\text{storage\_treatment}} = H^{\text{time}} \sum_{s,a,t} UTC^{\text{storage\_treatment}} ff_{s,a,t}^{\text{storage\_treatment}} \tag{51}$$

$$TransCost^{\text{treatment\_reuse}} = H^{\text{time}} \sum_{a,r,t} UTC^{\text{treatment\_reuse}} ff_{a,r,t}^{\text{treatment\_reuse}} \tag{52}$$

$$TransCost^{\text{treatment\_disposal}} = H^{\text{time}} \sum_{a,d,t} UTC^{\text{treatment\_disposal}} ff_{a,d,t}^{\text{treatment\_disposal}} \tag{53}$$

$$TransCost^{\text{total}} = TransCost^{\text{well\_storage}} + TransCost^{\text{storage\_treatment}} + TransCost^{\text{treatment\_reuse}} + TransCost^{\text{treatment\_disposal}} \tag{54}$$

Capital Cost. As discussed in section 3.1.2, the total capital cost for the TMD system is stated below.

$$CapCost^{\text{treatment}} = \sum_a 58.5A_{m,a} + \frac{\sum_{a,t} 1115F_{a,t}^{\text{treatment\_in}}}{|t|} \tag{55}$$

The capital costs for storage, reuse, and disposal units are given in eqs 56−58, which are taken from Lira-Barragan et al.[5]

$$CapCost^{\text{storage}} = K\Sigma_s[FC^{\text{storage}} y_s^{\text{storage}} + (VC^{\text{storage}} V_s^{\text{storage\_capacity}})] \tag{56}$$

$$CapCost^{\text{reuse}} = K\Sigma_r[FC^{\text{reuse}} y_r^{\text{reuse}} + (VC^{\text{reuse}} V_r^{\text{reuse\_capacity}})] \tag{57}$$

$$CapCost^{\text{disposal}} = K\Sigma_d[FC^{\text{disposal}} y_d^{\text{disposal}} + (VC^{\text{disposal}} V_d^{\text{disposal\_capacity}})] \tag{58}$$

where K is a factor used to annualize the inversion; FC^{storage}, FC^{reuse}, and FC^{disposal} are fixed charges included in the capital cost functions for storage units, reuse units, and disposal units, respectively; VC^{storage}, VC^{reuse}, and VC^{disposal} are the corresponding variable charges.

Profit. Given the unit profit from reusing water (UP^{reuse}), the total profit is presented in eq 59.

$$Profit^{\text{reuse}} = H^{\text{time}} \sum_{r,t} UP^{\text{reuse}} F_{r,t}^{\text{reuse\_in}} \tag{59}$$

Total Annual Cost (TAC). Thus, the total annual cost associated with the wastewater management can be presented as stated in eq 60:

DOI: 10.1021/acs.iecr.9b01553
Ind. Eng. Chem. Res. 2019, 58, 12097−12115

$$TAC = (Cost^{\text{treatment}} + Cost^{\text{disposal}} + TransCost^{\text{total}}) + (CapCost^{\text{treatment}} + CapCost^{\text{storage}} + CapCost^{\text{reuse}} + CapCost^{\text{disposal}}) - Profit^{\text{reuse}} \quad (60)$$

3.2. Model Predictive Control for Hydraulic Fracturing. In this section, the proposed novel MPC system is presented, as shown in Figure 5.

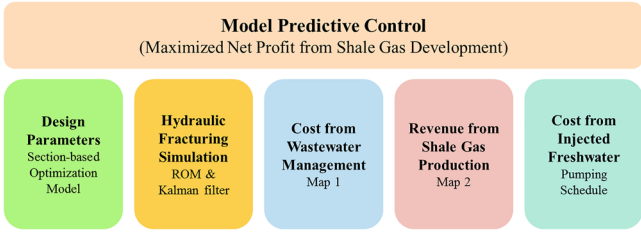

Figure 5. Schematic diagram for MPC system.

To combine the economic factors (i.e., revenue from shale gas production, cost from wastewater management, and cost from freshwater) with the simulation of the hydraulic fracturing process and design the integrated MPC system, a mapping-based technique is proposed. With the overall objective to maximize the net profit from the shale gas development, two maps are generated. When the optimization model developed in section 3.1 for wastewater management is applied, the minimized total cost is obtained based on a given flow rate and TDS concentration profiles of wastewater. Since these profiles are generated through the dynamic input−output model which correlates them with the injected fluid volume, different fluid volumes are implemented to generate the corresponding minimized costs. Thus, one map can be obtained to describe the minimized TAC associated with the wastewater management strategy. Then, by applying multiple random pumping schedules to the developed ROM and Kalman filter, their corresponding final fracture geometries are obtained. Thus, on the basis of the calculated propped fracture geometries and market price of shale gas, the second map is generated using CMG software, which describes the total revenue associated with the shale gas production. Along with the freshwater cost which is calculated by the pumping schedule, the MPC system is constructed. Particularly, the section-based optimization model is applied to provide the necessary design parameters used in the MPC formulation.

3.2.1. Section-Based Optimization Model. The section-based optimization model is adopted from Liu and Valko.[34] It is used to determine the optimum number of wells (n_c), number of fractures per well (n_r), and propped fracture half-length (x_f), which maximize the dimensionless productivity index (PI) for a given amount of injected proppant (M_{prop}).[34]

Defining that the large square drainage area for multistage fractured horizontal wells is the section, and drainage area for a single fracture is the subsection, the relationship between the section area (A_{section}) and the subsection area ($A_{\text{subsection}}$) is presented in eq 61.

$$A_{\text{section}} = A_{\text{subsection}} n_c n_r \quad (61)$$

Assuming that the created fractures will be of infinite conductivity and the injected amount of proppant is enough to ensure the enhanced permeability over the entire section, the overall dimensionless productivity of a section (J_D) is shown in eqs 62−64.

$$J_D = n_f J_{D,f}(A_r, I_x) \quad (62)$$

$$n_f = n_c n_r \quad (63)$$

$$A_r = \frac{n_r}{n_c}, \quad I_x = \frac{l_f}{n_r\sqrt{A_{\text{section}}}}, \quad l_f = \frac{M_{\text{prop}}}{\rho_p W_{\text{opt}} H_r} \quad (64)$$

where n_f is the total number of fractures in the section, $J_{D,f}$ is the dimensionless productivity index (PI) for a fracture, which is a function of aspect ratio (A_r) and penetration ratio (I_x); l_f is the total fracture length, M_{prop} is the total amount of injected proppant, ρ_p is the proppant particle density, W_{opt} is the minimum required average propped fracture width, and H_r is the reservoir thickness. Given that the values of M_{prop}, W_{opt}, H_r and A_{section} are available, the three decision variables mentioned above (n_c, n_r, x_f) can be determined.

Assuming the proppant bank will cover the optimum propped fracture half-length (x_f) with the equilibrium proppant bank height (h_{eq}), the desired average fracture width over the optimum propped fracture half-length ($W_{\text{avg,target}}$) is calculated as stated in eq 65.

$$W_{\text{avg,target}} = \frac{M_{\text{prop},f}}{2\rho_p h_{\text{eq}} x_f (1-\phi)} \quad (65)$$

where $M_{\text{prop},f}$ is the given injected proppant amount for one fracture, ϕ is the proppant bank porosity. When pumping is stopped, the fracturing fluid will leak off and the proppant will be trapped by fractured wells; this phenomenon is called fracture closure. Note that W_{opt} is the average fracture width at the end of fracture closure while $W_{\text{avg,target}}$ is the average fracture width at the end of pumping. One assumption is that over the course of fracture closure process, the average fracture width will decrease from $W_{\text{avg,target}}$ to W_{opt}.

3.2.2. Reduced-Order Model and Kalman Filter. By applying the proppant bank formation mechanism, a nonlinear high-fidelity model for a hydraulic fracturing process is developed by Siddhamshetty et al.[23] With the input/output simulation data generated by the high-fidelity model in which the input is the pumping schedule and the output is the final fracture geometry, a linear time-invariant state-space model of the hydraulic fracturing process is developed using the multivariable output error state-space (MOESP) algorithm. The model formulation is shown in eqs 66 and 67.

$$x(t_{k+1}) = Ax(t_k) + Bu(t_k) \quad (66)$$

$$y(t_k) = Cx(t_k) \quad (67)$$

where $u(t_k)$ is the input, $x(t_k)$ is the state, and $y(t_k)$ is the output at time point t_k. The parameters (A, B, C) are determined by the MOESP algorithm. Specifically, the input includes the flow rate $Q_0(t_k)$ and the proppant concentration $C_0(t_k)$ of the injected fracturing fluid at the wellbore. The output includes the average fracture width over the optimum fracture half-length $W_{\text{avg},x_f}(t_k)$, the fracture width at the wellbore $W_0(t_k)$, and the fracture length $L(t_k)$. Note that among the three output variables, the real-time measurements of $W_0(t_k)$ and $L(t_k)$ are assumed to be available during the operation of hydraulic fracturing.

To obtain the unmeasurable output variable, $W_{\text{avg},x_f}(t_k)$, a Kalman filter is developed. Equations 68−70 state that the

DOI: 10.1021/acs.iecr.9b01553
Ind. Eng. Chem. Res. 2019, 58, 12097−12115

Kalman filter is designed based on the obtained ROM and the available measurements as follows:

$$\hat{x}(t_{k+1}) = A\hat{x}(t_k) + Bu(t_k) + M(t_k)[y_m(t_k) - \hat{y}(t_k)] \quad (68)$$

$$M(t_k) = P(t_k)H^T[R(t_k) + CP(t_k)C^T]^{-1} \quad (69)$$

$$P(t_{k+1}) = [I - M(t_k)C]P(t_k) \quad (70)$$

where $u(t_k)$ is the input, $\hat{x}(t_k)$ and $\hat{y}(t_k)$ are the estimates of the state and output variables, $M(t_k)$ is the Kalman filter gain, and $P(t_k)$ is the covariance of the state estimation error. The Kalman filter allows the state estimates to be updated iteratively based on the available real-time measurements, which makes the state estimation more accurate.

3.2.3. Map 1. As mentioned, a dynamic input−output model for flowback water is developed based on field data to describe the relationship between the input (i.e., pumping schedules) and the output (i.e., flow rate and TDS concentration profiles of wastewater).

On the basis of the operational definition, flowback water is the wastewater which returns to the surface within the first few weeks after hydraulic fracturing is completed, and produced water is the wastewater generated in the production stage along with shale gas. Flowback water is characterized by a high flow rate and a low TDS concentration. Produced water, by contrast, returns to the surface with a high TDS concentration due to bringing the components associated with the formation and the entrapped fluid in the pore spaces. After hydraulic fracturing is completed, the pressure in the formation is gradually released along with time, and the injected fracturing fluid picks up inorganic constituents when residing downhole. Thus, the trend of continuously increasing TDS concentration and decreasing flow rate is predominant for wastewater. In this regard, we assume that the flow rate and TDS concentration can be represented by time-varying continuous variables. Since the characteristics of the wastewater would change little in the last few years as reported, natural logarithm equations are assumed to develop the input−output model by a regression technique.[35] Thus, the flow rate profile and the TDS concentration profile are formulated as stated in eqs 71 and 72, respectively.

$$F_{n,t}^{\text{well\_out}} = Q_n^{\text{injected}}(a \ln(t) + b), \quad \forall\, n \,\forall\, t \quad (71)$$

$$C_{n,t}^{\text{well\_out}} = c \ln(t) + d, \quad \forall\, n \,\forall\, t \quad (72)$$

where a, b, c, and d are parameters determined by the regression technique, and Q_n^{injected} is the total volume of injected fluid for fractured well n. Note that the flow rate profile changes with the volume of injected fluid, while the TDS concentration profile remains the same since it is assumed to be only a function of time.

By injecting fracturing fluids with different volumes, a variety of flow rate profiles can be generated. They are then used with the TDS concentration profile as the inputs to the wastewater management optimization model to compute the corresponding minimized TACs. Thus, a map is constructed that shows the TAC from the wastewater management process as a function of the volume of injected fracturing fluid for one fractured well. Note that to develop the map, it is assumed that all the wells are identical, and thus, the volume of injected fluid for each well can be denoted as Q^{injected}.

$$TAC = g(Q^{\text{injected}}) \quad (73)$$

It is noted that Q^{injected} can be calculated based on the pumping schedule, which provides the flow rate $(Q_0(t_k))$ and the proppant concentration $(C_0(t_k))$ of the injected fracturing fluid to create an half of the fracture. Assuming that Q^{injected}, refers to the volume of the injected pure water (i.e., injected freshwater) for one fractured well, it can be calculated using eq 74 as follows:

$$Q^{\text{injected}} = \Delta\left(\sum_k 2Q_0(t_k)(1 - C_0(t_k))\right)n_r \quad (74)$$

where Δ is the sampling time in the simulation work, n_r is the number of fractures per well determined by the section-based optimization model. Note that the amount of injected freshwater for each well is identical and should be the sum of the freshwater required for all the fractures inside.

REMARK 2. In this work, the flow rate and TDS concentration profiles are generated based on the ROM and Kalman filter discussed in section 3.2.2. In comparison to taking the sampled data from some reports directly, the main novelty here is to find the required fracturing fluid volume to create the desired fracture geometry (i.e., fracture length, height, and average width) which will affect the total shale gas production rate. Then, with the developed dynamic input−output model, the corresponding flow rate and TDS concentration profiles can be determined with the obtained injected fracturing fluid volume.

3.2.4. Map 2. As mentioned, the reservoir simulation software, CMG, is used to generate the shale gas production profile based on the final fracture geometry at the end of fracture closure.

With the component properties and the rock-fluid properties of a shale reservoir as well as the operation conditions, the numerical reservoir simulator of CMG is applied to model hydraulic fractures using one of its packages called GEM. Specifically, we focus on the modeling of one-wing fracture due to the symmetric nature of the bi-wing structure. Using the propped fracture geometry as the input, the shale gas production profile can be obtained. The total revenue from shale gas production ($TRSG$) for the shale reservoir can be calculated using eq 75.[36]

$$TRSG = \int_0^{t_b} (\overline{q}_0 r_0 (1 + I)^{-ct}) n_c \, dt \quad (75)$$

where $\overline{q}_0$ is the shale gas production rate for one fractured well, t_b is the well production time, I is the money discount rate, r_0 is the current market price of shale gas, c is the time constant, and n_c is the number of the wells determined by section-based optimization model. In this work, the parameters I and c are taken to be 0.1 and $\frac{1}{365}(1/\text{day})$, respectively.

The input to CMG-GEM is the propped fracture geometry (i.e., the fracture geometry at the end of fracture closure), which includes the average propped fracture width (W_{opt}), propped fracture half-length (L_f) and propped fracture height (H_r). Here, the propped fracture half-length for each fracture is calculated using eq 76 and $M_{\text{prop,frac}}$ is the final amount of the injected proppant for one fracture.

$$L_f = \frac{M_{\text{prop,frac}}}{\rho_p h_{\text{eq}} W_{\text{avg},x_f}(1 - \phi)} \quad (76)$$

DOI: 10.1021/acs.iecr.9b01553
Ind. Eng. Chem. Res. 2019, 58, 12097−12115

A set of different propped fracture geometries is used as the input to CMG-GEM to generate the corresponding shale gas production profiles with the associated revenue. Thus, a second map is developed, as presented in eq 77, where the total revenue ($TRSG$) obtained by selling shale gas produced is a function of the propped fracture geometries (W_{opt}, L_f, H_r).

$$TRSG = h(W_{\text{opt}}, L_f, H_r) = h(L_f) \tag{77}$$

In this study, we assumed that fracture propagation is confined within a layer so the propped fracture height does not change much, and the average propped fracture width is taken to be three times the diameter of proppant particles, which is used as the minimum required propped fracture width. Thus, the revenue only changes with the propped fracture half-length. Note that since all the wells are assumed to be identical, the fracture geometries and the corresponding shale gas production rate for each well are the same.

3.2.5. MPC Formulation. Since the volume of the injected freshwater for one well is determined based on the pumping schedule as stated in eq 74, the total freshwater cost (TFC) for the shale reservoir is obtained in eq 83 with given unit cost for freshwater (UC^{fresh}). Finally, the objective of the novel MPC system is formulated as in eq 78 to maximize the net profit associated with the shale reservoir development as follows:

$$\max_{\substack{C_{\text{stage},k},\ldots,C_{\text{stage},9}\\ Q_{\text{stage},k},\ldots,Q_{\text{stage},9}}} \quad TRSG - TAC - TFC \tag{78}$$

s.t. ROM & Kalman filter (79)

$$\hat{W}_0(t_k) = W_0(t_k),\ \hat{L}(t_k) = L(t_k) \tag{80}$$

$$TRSG = h(L_f) \tag{81}$$

$$TAC = g(Q^{\text{injected}}) \tag{82}$$

$$TFC = UC^{\text{fresh}}(Q^{\text{injected}} n_c) \tag{83}$$

$$L_f = \frac{M_{\text{prop,frac}}}{\rho_p h_{\text{eq}} \hat{W}_{\text{avg},x_f}(1-\phi)} \tag{84}$$

$$Q^{\text{injected}} = \Delta\left(\sum_k 2Q_{\text{stage},k}(1 - C_{\text{stage},k})\right) n_r \tag{85}$$

$$M_{\text{prop,frac}} = \Delta\left(\sum_{k=1}^{9} 2Q_{\text{stage},k} C_{\text{stage},k}\right) \tag{86}$$

$$C_{\text{stage},k-1+m} \le C_{\text{stage},k+m} \le C_{\max} \tag{87}$$

$$Q_{\min} \le Q_{\text{stage},k+m} \le Q_{\max} \tag{88}$$

$$M_{\text{prop,frac}} \le M_{\text{prop},f} \tag{89}$$

$$\hat{W}_{\text{avg},x_f} = W_{\text{avg,target}} = \frac{M_{\text{prop},f}}{2\rho_p h_{\text{eq}} x_f (1-\phi)} \tag{90}$$

$$m = 1, \ldots 9 - k \tag{91}$$

where eq 79 represents the ROM and Kalman filter developed in section 3.2.2. Equation 80 states that the Kalman filter is initiated by utilizing the real-time measurement of the fracture width at the wellbore ($W_0(t_k)$) and fracture length ($L(t_k)$) at each sampling time t_k, as initial conditions. Equations 81 and 82 are the two maps generated to calculate the total revenue from shale gas production, and the total annual cost from wastewater management. The two maps are based on the propped fracture half-length (L_f) and the volume of the injected freshwater (Q^{injected}) for one fractured well, which are calculated using eqs 84 and 85. It is noted that the number of fractured wells in the wastewater management optimization model is $N = n_c$. With the given unit cost (UC^{fresh}) for the freshwater required to be injected, the total cost for the freshwater (TFC) is calculated using eq 83. With $C_{\text{stage},k}$ and $Q_{\text{stage},k}$ representing the inlet proppant concentration and the inlet flow rate of fracturing fluid at the k^{th} pumping stage, the volume of injected pure water for one fractured well (Q^{injected}) and the amount of proppant injected to one well ($M_{\text{prop,frac}}$) during hydraulic fracturing are calculated using 85 and 86. Equations 87 and 88 are the constraints imposed on the flow rate and proppant concentration; in particular, the proppant concentration increases with time but it should not exceed the maximum. Since the average propped fracture width (W_{opt}) is fixed, with the assumption mentioned in section 3.2.1, the estimated average fracture width at the end of pumping ($\hat{W}_{avg,x_f}$) should be equal to the desired value ($W_{\text{avg,target}}$) and calculated as stated in eq 90. $M_{\text{prop},f}$ is the given amount of injected proppant for one fracture to make sure that the average fracture width will decrease to three times the diameter of proppant particles at the end of fracture closure. Equation 89 implies that the final injected proppant amount ($M_{\text{prop,frac}}$) could be less than the given value, $M_{\text{prop},f}$, due to a possible decrease in the volume of injected fracturing fluid.

In this work, since the inputs of the wastewater management optimization model are the flow rate and TDS concentration profiles, which are determined by the pumping schedule, hydraulic fracturing will directly affect the wastewater management. Although the cost associated with the wastewater management is always minimized and not directly sent back to the hydraulic fracturing model, since it is included in the MPC to maximize the net profit, wastewater management will also affect the hydraulic fracturing. Thus, the hydraulic fracturing process and the water management are simultaneously optimized to reach the maximized net profit.

REMARK 3. In this MPC, the linear ROM is used to approximate the nonlinear high-fidelity hydraulic fracturing model, and the Kalman filter is developed to estimate the unmeasurable average fracture width and initial states of the system, which will be used in the MPC to predict future state trajectories. When developing the ROM, the trained input profiles are selected within the range which can cover the entire range of operating conditions that are generally being considered in the field (i.e., the upper bound and lower bound on the flow rate and proppant concentration of injected fracturing fluid). Since these ranges are also included in the MPC formulation as the important constraints (i.e., eqs 87 and 88), the obtained ROM is always valid for this simulation work.

REMARK 4. In this work, the focus is to investigate the trade-off between the hydraulic fracturing and water management. Since the objective function of MPC is directly related to the economic performance for shale gas development and the regulation of fracture geometry to a desired value is included as one constraint (i.e., eq 90), this MPC can also be described as economic model predictive control (EMPC) which refers to a framework that integrates economic process optimization and process control.

4. CASE STUDY AND ANALYSIS

To demonstrate the performance of the proposed control framework, an example representing a typical hydraulic fracturing process in the horizontal wells taken from Siddhamshetty et al. is considered.[23] During the operation of hydraulic fracturing, the total amount of proppant available for

DOI: 10.1021/acs.iecr.9b01553
Ind. Eng. Chem. Res. 2019, 58, 12097−12115

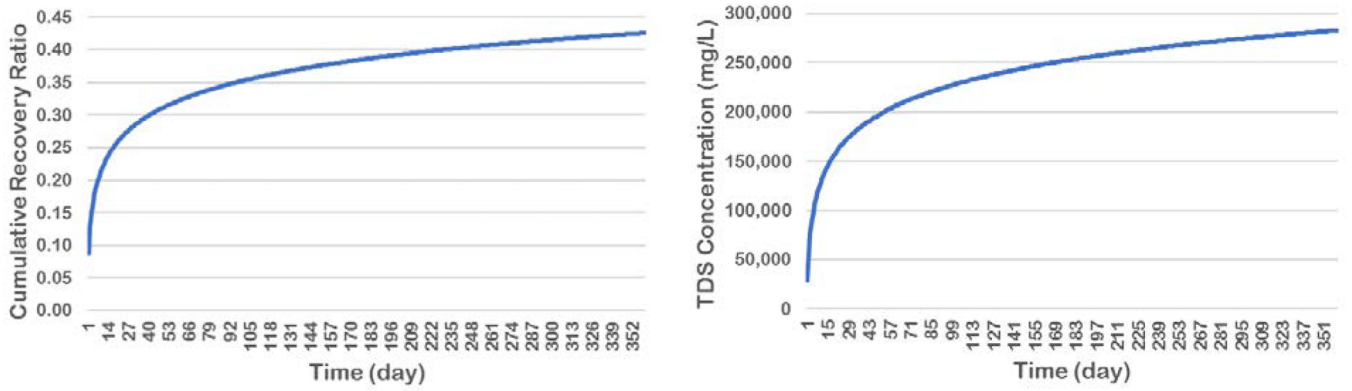

Figure 6. (a) Cumulative recovery ratio and (b) TDS concentration (mg/L) of wastewater.

the large square drainage area of $A_{section} = 2.59 \times 10^6$ m^2 is $M_{prop} = 2.41 \times 10^7$ kg, and the desired average fracture width at the end of pumping is $W_{avg,target} = 5.37$ mm. It is noted that in this study, we mainly focus on the net profit within the first production year.

As discussed in section 3.2.1, through the section-based optimization model, the fixed amount of proppant is converted to the total fracture length, which has to be satisfied to maximize the dimensionless productivity index (PI). Specifically, when the average propped width of $W_{opt} = 2.9$ mm and the reservoir thickness of $H_r = 60$ m are considered, the corresponding optimum number of wells (n_c), number of fractures per well (n_r), and propped fracture half-length (x_f) are found to be 6, 55, and 120 m, respectively. These are used as the key parameters in the subsequent optimization problem for wastewater management and the control system for hydraulic fracturing. Details of the solution are provided in Table S1 in the Supporting Information.

4.1. Optimization of Wastewater Management. *4.1.1. Dynamic Input−Output Model.* To obtain the flow rate profile and TDS concentration profile of the wastewater recovered within the first year, a dynamic input−output model is developed based on the field data taken from the information provided by Hayes et al.[35] The field data are provided in Tables S2 and S3. In the report, the sampled data are obtained from 19 locations within the Marcellus Shale Region, presenting the volume of injected fracturing fluid, and the cumulative volume of the flowback water recovered on day 1, 5, 14, and 90 (since the completion of hydraulic fracturing) as well as the corresponding TDS concentration.

To effectively develop an input−output model, some assumptions are made. First of all, the fact that the regional characteristics of flowback water can vary significantly from one place to another is neglected. Second, only the TDS coming from the shale formation after well completion is considered. Thus, the TDS concentration on day 0 is assumed to be negligible. Third, the injected fluid is assumed to be pure water. Focusing on the horizontal drilling data from the report,[35] the sampled data from the location C, D, E, F, G, K, M, O is used to develop the input−output model describing the flowback water volume and TDS concentration with time. With the assumptions mentioned above, the cumulative volume of flowback water is a function of the volume of injected fluid and time, while the TDS concentration is only a function of time. To simplify the model, we considered the recovery ratio instead of the cumulative volume; in particular, the recovery ratio is defined as the ratio of the generated wastewater volume to the injected fluid volume, as shown in eq 92. Using a regression technique, the natural logarithm function is applied to represent the relationship between the characteristics of flowback water and time, which is shown in Figure S1. The corresponding regression model is presented as follows:

$$y_{n,t}^{well\_out} = \frac{Q_{n,t}^{well\_out}}{Q^{injected}}, \quad \forall\, n, \forall\, t \in [1, 90] \tag{92}$$

$$y_{n,t}^{well\_out} = 0.0575 \ln(t) + 0.0877, \quad \forall\, n, \forall\, t \in [1, 90] \tag{93}$$

$$C_{n,t}^{well\_out} = 43134.79 \ln(t) + 28925.13, \quad \forall\, n, \forall\, t \in [1, 90] \tag{94}$$

where t is in days from the moment the hydraulic fracturing is completed, $Q^{injected}$ is the total volume of the injected water for one fractured well, $Q_{n,t}^{well\_out}$ is the cumulative volume of the generated wastewater in well n in time period t and $y_{n,t}^{well\_out}$ and $C_{n,t}^{well\_out}$ are the cumulative recovery ratio and the TDS concentration in well n in time period t, respectively. It is noted that since the input−output model is developed based on the regression technique, the obtained model's validity should be constrained by the sampled data; specifically, the developed model can be applied within the range from approximate 20 000 to 150 000 BBL for the volume of injected fracturing fluid.

Assuming that the returned formation water is neglected and the characteristics of the flowback water (i.e., essentially produced water) follow the trend over the first 90 days, the cumulative recovery ratio profile and the TDS concentration profile of the wastewater recovered over the first year are shown in Figure 6.

The recovery ratio on day 14 is around 0.24 which is close to the average recovery ratio provided in the report. On day 360, it reaches nearly 0.42 which is comparable to the recovery ratio at location D and E on day 90 from Hayes et al.[35] On the other hand, the TDS concentration on day 90 is 220 000 mg/L and it reaches 280 000 mg/L on day 360 which is close to the median TDS values of 278 000 mg/L presented in the work of Rowan et al.[37]

Thus, once the flow rate and TDS concentration profiles are obtained from the data-based dynamic input−output model, they will be used as the inputs to the wastewater management optimization model. To verify the proposed MINLP optimization model's effectiveness and reliability, two case studies are presented. Specifically, Case 1 refers to a small-scale management process while Case 2 refers to a large-scale one which mimics a field case that contains multiple wells.

DOI: 10.1021/acs.iecr.9b01553
Ind. Eng. Chem. Res. 2019, 58, 12097−12115

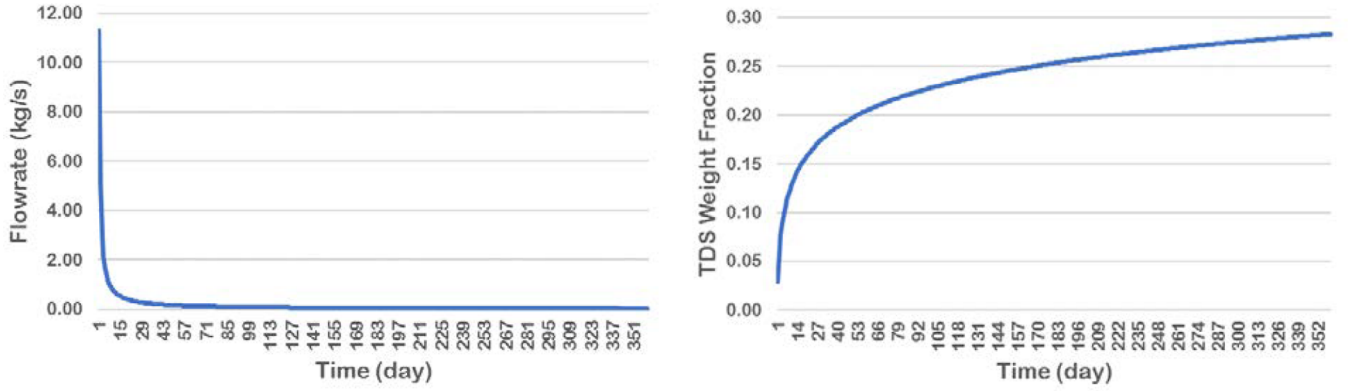

Figure 7. (a) Flow rate (kg/s) and (b) TDS weight fraction of wastewater.

REMARK 5. The assumptions made in developing the dynamic input−output model can be relaxed. As for the first assumption, a detailed model with clear physical meaning can be developed based on some shale formation properties such as the permeability and porosity, which is able to explicitly interpret the significant difference in the wastewater characteristics between different locations. As for the second assumption, since the TDS concentration is generally used to determine the quality of wastewater and the data on day 0 represents the additives in the fracturing fluid, it is appropriate to assume that only the TDS coming from the shale formation is considered. As for the third assumption, it can be relaxed if the proppant concentration of the injected fracturing fluid is available; otherwise, it is an appropriate assumption since more than 90% of the fracturing fluid is pure water.

4.1.2. Case Study 1. In Case 1, we considered one fractured well, one wastewater storage, one TMD system, one reused water tank, and one rejected water tank. The time horizon is one year, and the unit time period is a day. The main objective is to cost-effectively manage the wastewater generated from the post-fracturing process (i.e., after hydraulic fracturing is completed).

With the developed input−output model, the cumulative volume of wastewater generated within the first year can be obtained when the volume of injected fluid is given; then, it can be converted to the flow rate in each day. The TDS concentration of the wastewater within the first year is also obtained, and it can be converted to the weight fraction by assuming that the wastewater density is constant as 1000 kg/m^3. In this case, the volume of injected fluid is considered to be 70 000 BBL. Thus, the flow rate and the TDS weight fraction profiles are generated as shown in Figure 7.

The parameters and the cost coefficients used in the wastewater management optimization model are given in Table S5. Since we only considered a single unit for each process in Case 1, the binary variables mentioned in section 3.1.1 can be removed, which transforms the model from MINLP to NLP. The resultant NLP model consists of 12 977 continuous variables and 18 379 equations. Implemented in the General Algebraic Modeling System (GAMS), it is solved using a global optimization solver (ANTIGONE[38]) on an Intel 3.4 GHz Core i7 CPU machine with 16 GB memory.

To deal with the large computational requirements due to the excessive input data points, we combined the data by month and regenerate 12 data points (i.e., in months) instead of 360 data points (i.e., in days). Using the combined data as the input, the complexity of the NLP model is effectively reduced as observed in Table 1. It is noted that since the solver ANTIGONE always reformulates the given model and detects the special structure before initializing the branch-and-bound global optimization algorithm, the provided computational statistics are obtained after the preprocessing.[38] Through the solver ANTIGONE, the global optimal solution for wastewater management in Case 1 is obtained. The results are provided in Tables S6 and S7. Some results for design variables and costs are presented in Table 2.

Table 1. Comparison of the Computational Statistics in Case 1

	360 data points	combined 12 data points
no. of continuous variables	4320	144
no. of nonconvex nonlinear equations	5033	161
no. of nonlinear terms	4317	141
CPU time (s)	no solution returned	42.52

Table 2. Design Variables and Costs for Wastewater Management in Case 1

variable	value
capacity of wastewater storage (kg)	2.89×10^6
capacity of reused water tank (kg)	2.62×10^5
capacity of rejected water tank (kg)	2.31×10^5
membrane area of TMD system (m^2)	393
profit from reusing water ($/year)	5,890
TOC ($/year)	63,106
TCC ($/year)	37,565
TAC ($/year)	94,781

As shown in Table 2, the optimized wastewater management associated with Case 1 leads to a total annual cost of $94,781, with $63,106 in operating cost, $37,565 in capital cost, and $5,890 from utilization of the reused water during the first year. As shown in Table S6, it is observed that the costs associated with the treatment unit account for a large proportion in both the operating and capital cost. Specifically, the total cost associated with the TMD system, which is $44,761, makes up around 47% of the total annual cost. Because of the constraints considered in this work that the complete rejection is assumed in the TMD system and all the generated wastewater is required to be treated before the next step, the TMD system is the most important part that contributes to the total cost in wastewater management.

DOI: 10.1021/acs.iecr.9b01553
Ind. Eng. Chem. Res. 2019, 58, 12097−12115

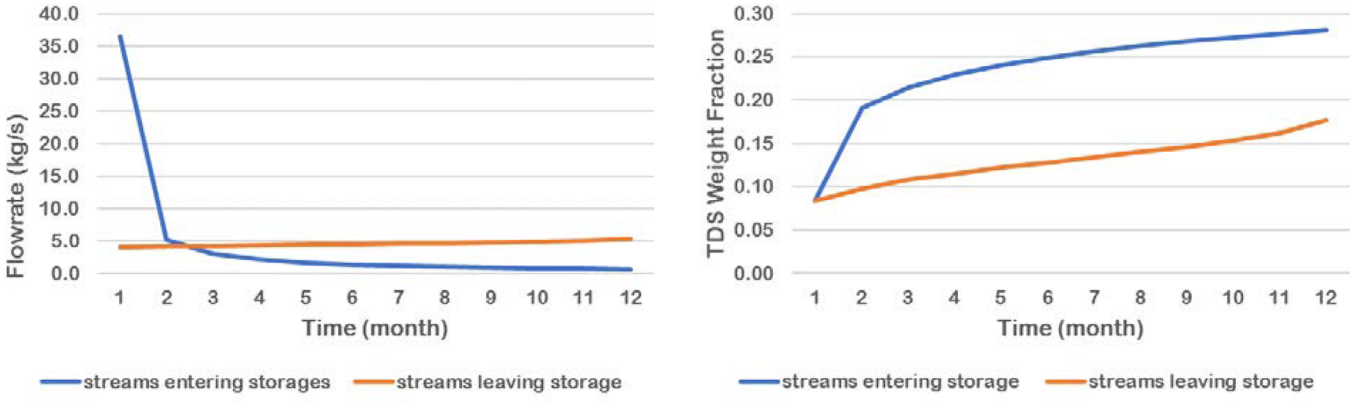

Figure 8. Comparison of (a) the flow rate (kg/s) and (b) the TDS weight fraction of the streams entering the storage and leaving the storage.

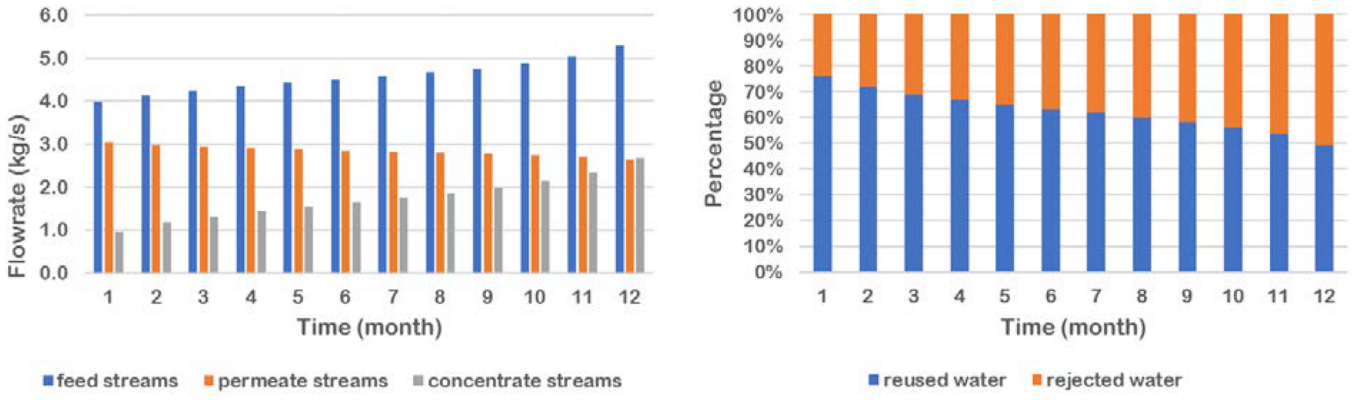

Figure 9. (a) Flow rate (kg/s) of the feed, permeate, and concentrate streams and (b) percentage of reused and rejected water.

As mentioned, the initially generated water is characterized by a high flow rate and a low TDS concentration. Then, the flow rate decreases while the TDS concentration increases over time. Thus, there are two extreme approaches to manage the wastewater. One is to treat nearly all of the wastewater generated in each month. In this approach, during the first few months, most of the wastewater can be treated with a relatively low operating cost because of the low TDS concentration. Although the unit operating cost becomes high with the TDS concentration, the total operating cost required during the last few months is not high since the flow rate is insignificant. The only problem is that since the flow rate in the first month is extremely high, the membrane area required in the TMD system should be large, which in turn increases the capital cost in the treatment unit. Another approach is to store most of the wastewater generated in the first few months. Thus, the wastewater recovered in different time periods can be blended in the storage unit. Since the volume of the initially generated wastewater is extremely large, even though the TDS concentration of the wastewater in the last few months is high, the final TDS concentration of the mixture leaving the storage can be reduced, which decreases the unit operating cost. The only problem is that the required capacity of the storage unit should be large, which in turn increases the capital cost in the storage unit.

On the basis of the results for the flow rate and TDS weight fraction for the streams around units, which are shown in Table S7, the second method is chosen in this Case 1 and the comparisons of the flow rate and the TDS weight fraction before and after the storage unit are presented in Figure 8. This illustrates that, with the storage unit, the flow rate of the streams leaving the storage is nearly the average value and the TDS weight fraction of the mixed streams is nearly reduced by half. Even though in the first month, nearly 90% of the generated wastewater is stored, which makes the capacity of the storage really large, it is still preferred since the capital cost in the storage unit is much less than the capital cost in the TMD system.

As for the performance of the TMD system, the comparisons of the flow rate in the permeate streams and concentrate streams are presented in Figure 9. Since the complete rejection in the permeate side is assumed and the weight fraction of TDS in the concentrate streams should not exceed 0.35, the optimal condition should be achieved by treating the wastewater as much as possible. On the basis of the optimal solution, the TDS weight fractions of the concentrate streams in all time periods are 0.35, reaching the upper limit. As time goes on, the flow rate of the treated water entering the disposal unit increases while the flow rate of the treated water entering the reuse unit decreases, which avoids the increase in the membrane area required. Specifically, at the beginning, around 76% of the wastewater can be reused, but at the end, only 49% can be reused.

4.1.3. Case Study 2. Another large-scale case study (Case 2) is presented considering six wells, which is the optimum number of wells determined by the section-based optimization method in section 3.2.1. Meanwhile, multiple storage, reuse, and disposal units are available to handle the wastewater generated from multiple wells (i.e., it is assumed that four wastewater storages, two reused water tanks and two rejected water tanks are available). Unlike the mentioned pumping schedule, which is used for hydraulic fracturing operation to achieve the desired

DOI: 10.1021/acs.iecr.9b01553
Ind. Eng. Chem. Res. 2019, 58, 12097−12115

fracture geometry, the scheduling problem which is generally considered in the context of upstream oil and gas application refers to a schedule (i.e., sequence) of drilling wells and performing hydraulic fracturing jobs. In this work, we do not actually investigate the optimum schedule for the six wells to be fractured but have a brief discussion based on the results from one trivial schedule. That is, all of the six wells were fractured at the same time. Note that the time horizon considered is still one year. With the parameters provided in Table S5, the resultant MINLP optimization model is solved through ANTIGONE and the optimal results are provided in Tables S8 and S9. Some important results are presented in Table 3. Also, the results obtained by multiplying the results from Case 1 by six are also provided for comparison. Note that by considering the situation with single fractured well and multiple other units available, this MINLP optimization model is verified since the same results as the ones in Case 1 are obtained.

Table 3. Design Variables and Costs for Wastewater Management in Case 2

variable	Case 2	Case 1 × 6
computational time (s)	10,831	43[a]
optimum number of wastewater storages	2	1
optimum number of reused water tanks	1	1
optimum number of rejected water tanks	1	1
capacity of wastewater storage (kg)	5.21×10^6; 1.20×10^7	1.73×10^7; –
capacity of reused water tank (kg)	1.573×10^6	1.572×10^6
capacity of rejected water tank (kg)	9.48×10^5	1.39×10^6
membrane area of TMD system (m^2)	2357.5	2355.7
capital cost for storage unit ($/year)	12,841	16,932
capital cost for treatment unit ($/year)	168,500	168,398
capital cost for reuse unit ($/year)	1,991	6,990
capital cost for disposal unit ($/year)	6,480	33,072
TAC ($/year)	533,112	568,686

[a]Computational time is not multiplied by six.

As shown in Table 3, as compared to the results from Case 1, the obtained capacities and membrane area become really large (i.e., nearly six times the capacity in Case 1). However, with the cost coefficients applied in the capital cost formulations for storage, reuse, and disposal units (i.e., eqs 56–58), the changes in the corresponding capital costs are relatively small.

In this work, since it is assumed that all the reused water is directly sold in the market for profit instead of being reintroduced for other wells to create fractures, applying different schedules will only directly affect the wastewater management but not the hydraulic fracturing process. Note that the total shale gas production may change if the time horizon is extended due to the schedule or a higher net profit can be achieved through the MPC system. When applying different schedules to create the multiple wells, since the flow rate and TDS concentration of wastewater collected each day depend on the schedule of wells, the capacity of the storage, reuse, and disposal units as well as the membrane area of the TMD system will change and thus the total capital cost will change. However, since the number of wells is fixed and all six wells have same flow rate and TDS concentration profiles, the total volume of generated wastewater is independent of well schedule, and thus, the total operating cost will not change.

In this work, considering that the computational cost in Case 2 is much higher (i.e., 10,831 s) and the fact that the final simulation results highly depend on the schedule implemented for the multiple wells, we decide to focus on one fractured well to demonstrate the proposed framework.

4.2. Modeling of the Hydraulic Fracture. As mentioned, the square drainage area is $A_{section} = 2.59 \times 10^6$ m^2. On the basis of the section-based optimization method, the number of wells and the number of fractures in one well were determined to be 6 and 55, respectively. Thus, the length of a side of the section is 1609.35 m and the section is divided into 330 subsections using eq 61. For each subsection, the length is 268.22 m and the width is 29.26 m. Assuming the fracture height is the same as the reservoir thickness H_r = 60 m, the numerical model of the one-wing fracture is designed with a dimension of 29.26 m × 135 m × 60 m. Since the optimum propped fracture half-length is x_f = 120 m and the average propped width is W_{opt} = 2.9 mm, the dimension is refined in the I and J direction and the resulting

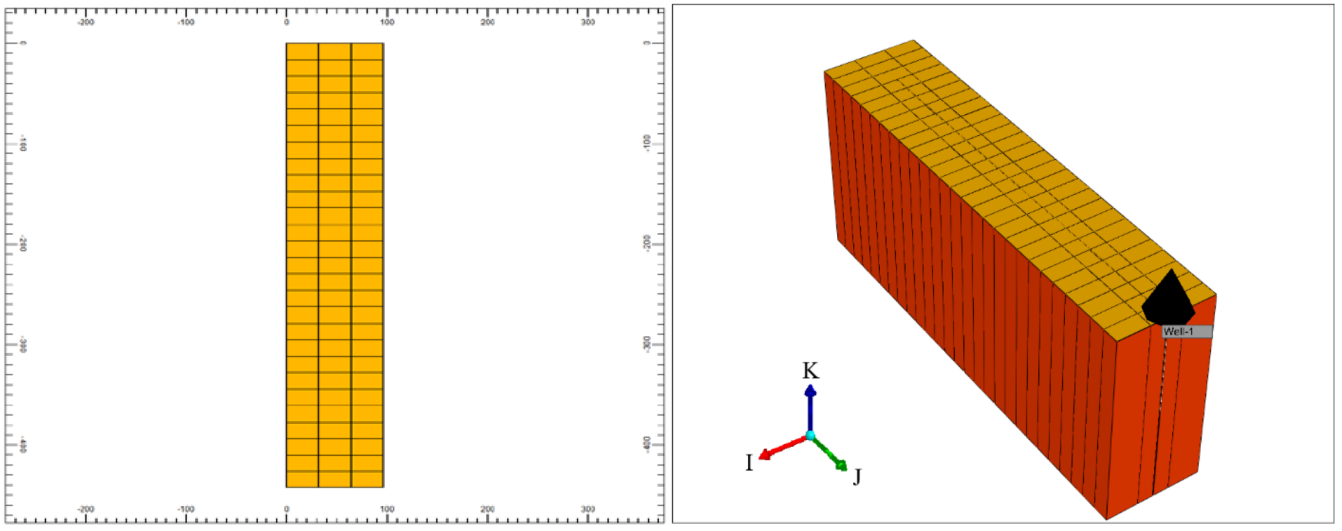

Figure 10. (a) 2D model and (b) 3D model of the one-wing fracture in CMG.

DOI: 10.1021/acs.iecr.9b01553
Ind. Eng. Chem. Res. 2019, 58, 12097–12115

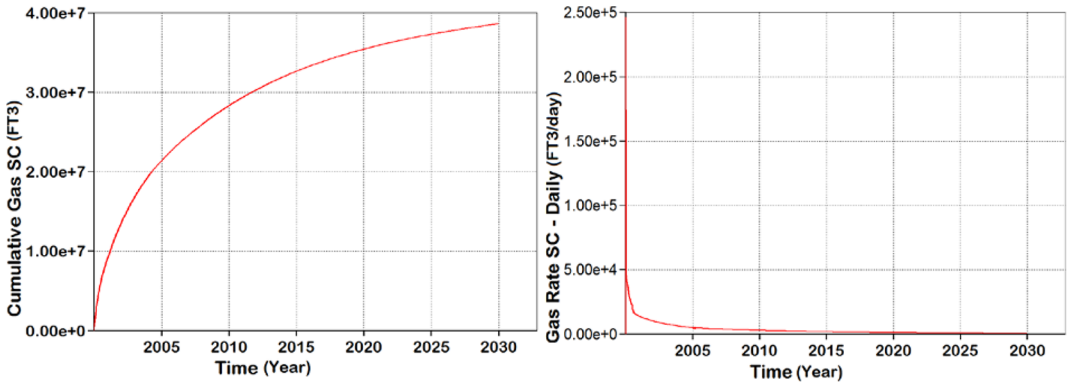

Figure 11. (a) Cumulative gas prodution (FT^3) and (b) gas flow rate (FT^3/day) for the 120 m one-wing fracture.

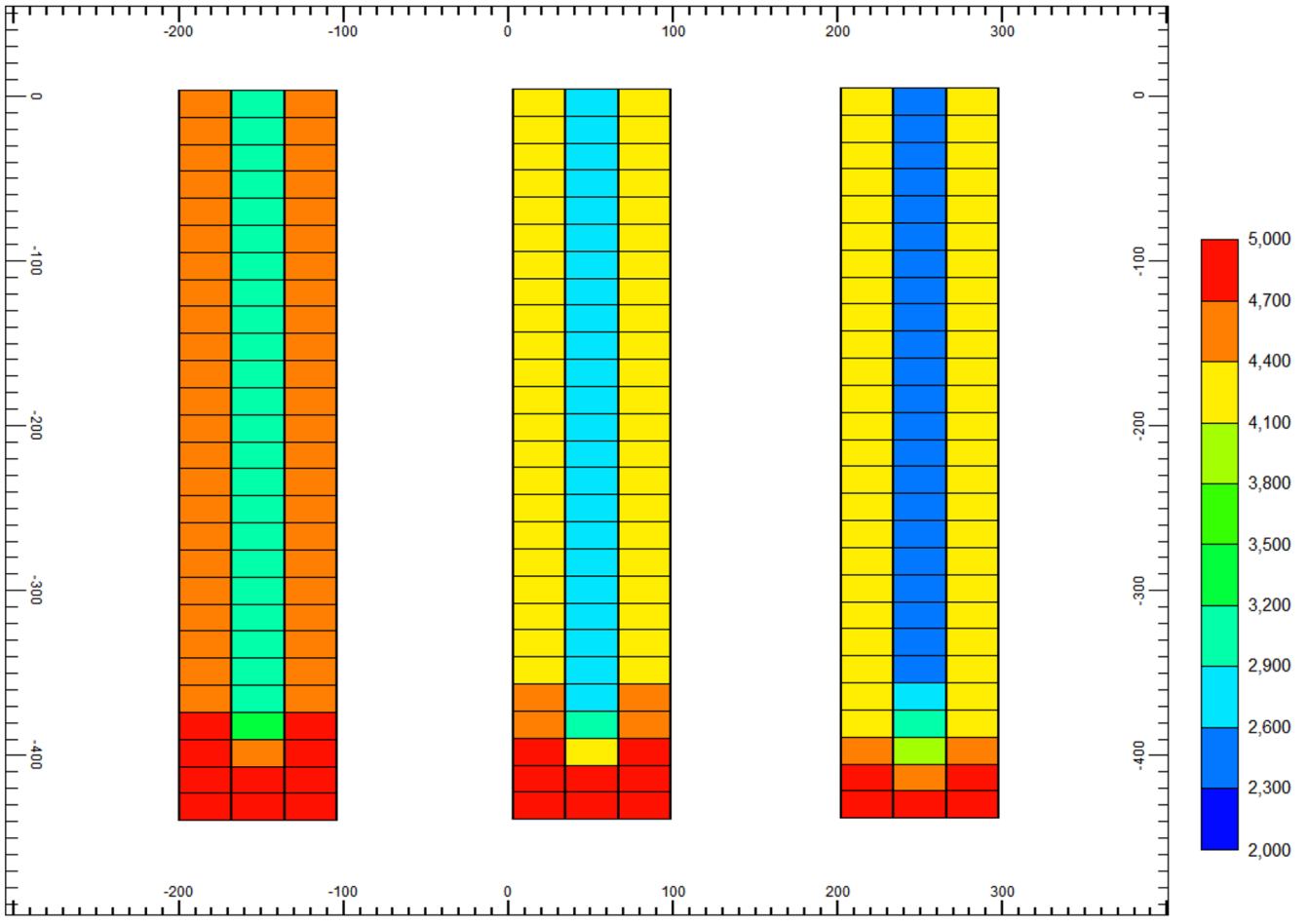

Figure 12. Pressure distribution after (a) 8 months; (b) 12 months; (c) 16 months production.

dimension of each grid is 9.75 m × 5 m × 60 m. Figure 10 represents the 2D and 3D model of the one-wing fracture. As shown in the 3D model, the black line along the J coordinate but in the opposite direction represents the fracture with the desired geometry.

The detailed shale and fracture properties of the Marcellus Shale well, which are used for the simulation work in CMG, are provided in Table S10. With the given parameters, when the propped fracture half-length is 120 m, the cumulative shale gas production profile and the shale gas flow rate profile for the one-wing fracture model are obtained as presented in Figure 11. Note that the generated profiles through CMG are the production forecasts for a thirty-year period. Considering that the market selling price of the shale gas production is $3/MMBTU, the revenue from selling produced shale gas is calculated. Specifically, when the propped fracture half-length is 120 m, the total shale gas production per well within the first year is 1003.2 $MMFT^3$ and the corresponding total revenue is $3.13 MM. Comparing with the field data provided by Yu et al.,[39] which is about 500 $MMFT^3$, the main reason for the difference is that the number of fractures per well in our case is nearly twice as many as the one in their work.

On the other hand, Figure 12 shows the pressure distributions for the same fracture presented in Figure 10 after 8, 12, and 16

DOI: 10.1021/acs.iecr.9b01553
Ind. Eng. Chem. Res. 2019, 58, 12097−12115

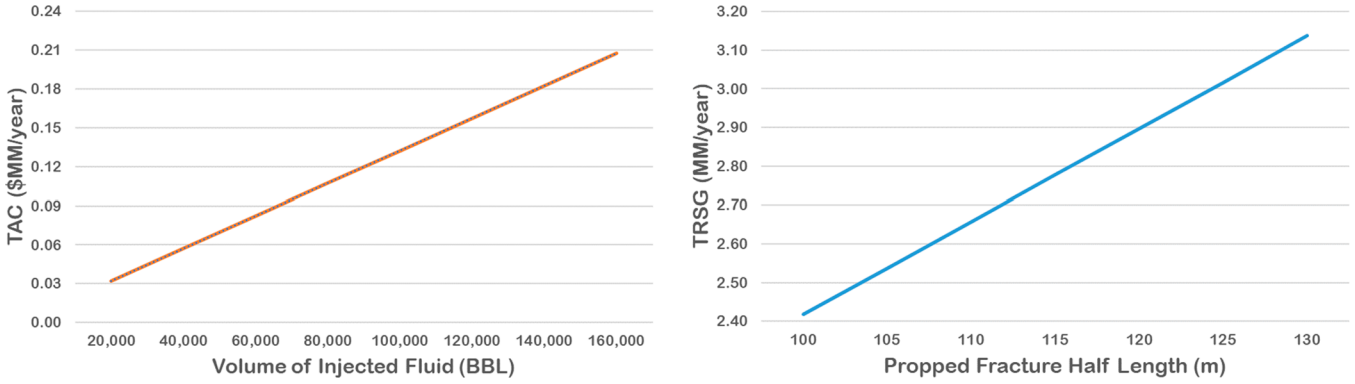

Figure 13. Maps from (a) optimization of wastewater management and (b) CMG reservoir simulation for different scenarios.

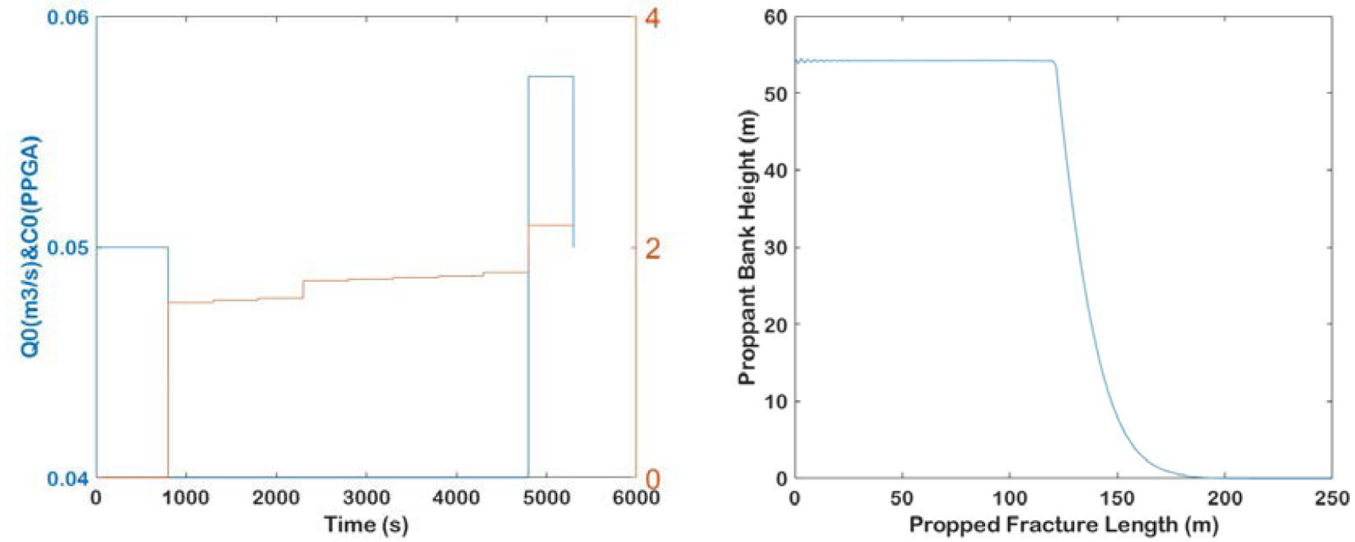

Figure 14. (a) Optimal pumping schedule and (b) proppant bank height profile.

months of field production. When the fracture is initially created, the pressure from the trapped oil and gas around the fracture is high. As time goes on, the pressure around the fracture will decrease continuously since the oil and gas are extracted. Generally, if the oil and gas pressure is high enough, there will be no interaction between the neighboring fractures. It is observed in Figure 12 that the pressure at the edge of the subsection is still as high as around 4300 psi at t = 12 months. Note that the initial reservoir pressure is 5024 psi as given in Table S10. Thus, it illustrates that the interaction can be neglected and it is feasible to approximate the total shale gas production by the simulation result from the one-wing fracture model multiplied by the number of one-wing fractures.

4.3. Proposed Mapping-Based Control of Hydraulic Fracturing. *4.3.1. Construction of Maps.* In the modeling of wastewater management, it is observed that the accumulative recovery ratio profile and the TDS weight fraction profile are fixed since they are only a function of time as shown in eqs 93 and 94. However, when the volume of injected fracturing fluid changes, the flow rate of the generated wastewater in each day changes as well as the associated total annual cost. In this regard, a series of injected fracturing fluid volumes are applied to the optimization model to generate input/output data, some of which are presented in Table S4. Then, the map representing the relationship between the minimized total annual cost and the volume of injected fluid as generated is shown in Figure 13.

In the modeling of the hydraulic fracture, assuming the reservoir parameters and the operating conditions are constant, the shale gas production is a function of the propped fracture geometry. Since the propped fracture height is assumed to be the same as the reservoir height and the average propped width is fixed at its optimum value, the gas production changes only with the propped fracture half-length. In this regard, a series of propped fracture half-lengths are applied to CMG to generate input/output data, some of which are presented in Table S11. The map representing the relationship between the total revenue from selling produced shale gas and the propped fracture half-length as generated is shown in Figure 13.

The relationships shown in Figure 13 which are based on a simple linear regression method, are presented using eqs 95 and 96, which are then used in the MPC formulation.

$$TAC = (1.2512Q^{\text{injected}} + 7200) \times 10^{-6} \quad (95)$$

$$TRSG = 0.0240x_f + 0.0198 \quad (96)$$

4.3.2. Model-Based Feedback Controller. In this reservoir example, the given total proppant amount is $M_{\text{prop}} = 2.409 \times 10^7$ kg, and the optimum propped fracture half-length is $x_f = 120$ m. Thus, the amount of the proppant injected for one fracture is $M_{\text{prop},f} = 7.3 \times 10^4$ kg. Provided that the proppant particle density is ρ_p = 2648 kg/m^3, proppant bank porosity is ϕ = 0.61, and equilibrium proppant bank height is h_{eq} = 54 m, the optimal

DOI: 10.1021/acs.iecr.9b01553
Ind. Eng. Chem. Res. 2019, 58, 12097−12115

average fracture width at the end of pumping is calculated to be $W_{avg,target}$ = 5.37 mm using eq 90. In the closed-loop simulation, the pad time is fixed to be 800 s, during which water is injected without proppant. The fracturing fluid is injected following the injection of pad; meanwhile, the control framework and the Kalman filter are initialized. The whole operation process is divided into nine stages, and the operation time in each stage is 500 s. In each simulation period, the real-time measurements of the fracture width at the wellbore and the fracture length are known beforehand and then used to estimate the unmeasurable average fracture width through the Kalman filter. At the same time, the flow rate and proppant concentration in each stage are determined by solving the optimization problem to maximize the net profit. This procedure will be repeated until the end of the hydraulic fracturing process. Since the Kalman filter is updated iteratively based on the difference between the predicted value and the measured value, the estimated average fracture width becomes more accurate; otherwise, its measurement is not available.

Applying the proposed MPC formulation discussed in section 3.2.5 and assuming that the unit cost of the freshwater (UC^{fresh}) is the same as the selling price of the reused water (UC^{reuse}) provided in Table S5 gives the pumping schedule and proppant bank height that are shown in Figure 14. It is observed that the flow rate of the injected fracturing fluid is always at the minimum level, except for in the last stage, while the proppant concentration monotonically increases and eventually reaches the maximum in the last stage. This pumping schedule helps reduce the volume of the injected freshwater while achieving the uniform proppant bank height across the desired optimum propped fracture half-length. With the obtained pumping schedule, the corresponding net profit from one horizontal well for the first year is about $2.703 MM. Other details are provided in Table 4.

Table 4. Closed-Loop Simulation Results for One Horizontal Well

variable	Siddhamshetty et al.[23]	our work ($M_{prop,f}$ = 36500)	our work ($M_{prop,f}$ = 34700)
proppant amount for half-fracture (kg)	36500	36500	34700
propped fracture half-length (m)	121.8	121.8	115.8
injected pure water volume (BBL)	166792	148692	139651
revenue from shale gas ($MM/year)	2.943	2.943	2.800
TAC from wastewater management ($MM/year)	0.216	0.193	0.182
cost from freshwater ($MM/year)	0.053	0.047	0.044
net profit ($MM/year)	2.674	2.703	2.574

For comparison purposes, the total revenue, total cost associated with wastewater management and injected freshwater are calculated based on the pumping schedule provided by Siddhamshetty et al.[23] It shows in Table 4 that, with the proposed control framework, a nearly 11% reduction in the total volume of the injected freshwater is achieved, which results in the net profit from one fractured well increasing by $0.029 MM. In addition, another case with 5% reduction in the total amount of proppant is also presented in Table 4. As shown, when the proppant amount is less, both the propped fracture half-length and injected freshwater amount decrease. Thus, the total revenue as well as the total cost from managing wastewater and from purchasing freshwater decreases. Since the change in the revenue is much more than that of the cost, the net profit is reduced. Particularly, the obtained net profit, which is $2.095 MM, is close to the net profit from Siddhamshetty et al.,[23] requiring nearly 5% less amount of the injected proppant and 16% less volume of the injected freshwater.

REMARK 6. The proposed framework is also applicable for a horizon with more than one year, such as 10 years, which is usually considered in the literature. Generally speaking, nearly 10−25% of the total wastewater production of a well over 10 years is generated during the first 3 months as flowback water while 20−50% is generated during the first 6 months.[40] However, with different unconventional basins, the total generated wastewater volume can be significantly different.[41] Also, due to the extension of production period (i.e., from 1 year to 10 years), the total shale gas production will change significantly. Thus, the final simulation results may change. In order to apply the proposed framework for 10 years, the flow rate and TDS concentration profiles of wastewater generated after the first year are required.

5. CONCLUSION

In this work, a novel closed-loop control framework has been proposed for shale gas development utilizing maps that describe the total annual cost of wastewater management and the total revenue from shale production as functions of the amount of freshwater injected and the propped fracture geometry, respectively. The goal is to balance a trade-off between hydraulic fracturing and water management by manipulating the pumping schedule. As a result, to inject the designated amount of proppant with less water, the volume of the freshwater injected was reduced by 11% while the desired fracture geometry was still achieved, leading to the theoretical maximum productivity. Once the hydraulic fracturing operation was completed, the generated wastewater was effectively treated by the TMD system, and 62% of the treated wastewater was sold in the market for reuse. To reduce the high cost associated with the treatment process, the initially generated wastewater was stored and then blended with the wastewater generated later, which allowed the TMD system to handle the wastewater with a smaller membrane area required. Considering that the reused water can be directly injected to other wells to further reduce the freshwater consumption in another hydraulic fracturing operation, future work will study the potential benefit of reintroducing the treated water. Future work can also be planned that considers multiple treatment technologies and quantitatively studies the environmental footprint of shale gas development.

■ ASSOCIATED CONTENT

Supporting Information

The Supporting Information is available free of charge on the ACS Publications website at DOI: 10.1021/acs.iecr.9b01553.

Nomenclature; section-based optimization model; dynamic input-output model; wastewater management model; single hydraulic fracture model; references (PDF)

DOI: 10.1021/acs.iecr.9b01553
Ind. Eng. Chem. Res. 2019, 58, 12097−12115

AUTHOR INFORMATION

Corresponding Author

*E-mail: kwonx075@tamu.edu.

ORCID

Joseph Sang-Il Kwon: 0000-0002-7903-5681

Notes

The authors declare no competing financial interest.

ACKNOWLEDGMENTS

The authors gratefully acknowledge financial support from the National Science Foundation (CBET-1804407), the Artie McFerrin Department of Chemical Engineering, and the Texas A&M Energy Institute.

REFERENCES

(1) *Annual energy outlook 2018 with projections to 2050*; U.S. Energy Information Administration, 2018.

(2) Wang, Z.; Krupnick, A. A retrospective review of shale gas development in the United States: What led to the boom? *Econ. Energy Environ. Policy* **2015**, *4* (1), 5−18.

(3) Hughes, J. D. Energy: A reality check on the shale revolution. *Nature* **2013**, *494* (7437), 307.

(4) Acharya, H. R.; Henderson, C.; Matis, H.; Kommepalli, H.; Moore, B.; Wang, H. Cost effective recovery of low-TDS frac flowback water for re-use. *DOE Report DE-FE0000784* **2011**, 100.

(5) Lira-Barragaén, L. F.; Ponce-Ortega, J. M.; Guilleén-Gosaélbez, G.; El-Halwagi, M. M. Optimal water management under uncertainty for shale gas production. *Ind. Eng. Chem. Res.* **2016**, *55* (5), 1322−1335.

(6) Karapataki, C. *Techno-economic analysis of water management options for unconventional natural gas developments in the Marcellus Shale*. Ms. Thesis, Massachusetts Institute of Technology, 2012.

(7) Dunn, S. Fracking 101: Breaking down the most important part of today's oil, gas drilling. *The Tribune*; Greely and Weld County: CO, 2016.

(8) Yang, L.; Grossmann, I. E.; Manno, J. Optimization models for shale gas water management. *AIChE J.* **2014**, *60* (10), 3490−3501.

(9) Yang, L.; Grossmann, I. E.; Mauter, M. S.; Dilmore, R. M. Investment optimization model for freshwater acquisition and wastewater handling in shale gas production. *AIChE J.* **2015**, *61* (6), 1770−1782.

(10) Gao, J.; You, F. Optimal design and operations of supply chain networks for water management in shale gas production: MILFP model and algorithms for the water energy nexus. *AIChE J.* **2015**, *61* (4), 1184−1208.

(11) Blewett, T. A.; Weinrauch, A. M.; Delompré, P. L.; Goss, G. G. The effect of hydraulic flowback and produced water on gill morphology, oxidative stress and antioxidant response in rainbow trout (Oncorhynchus mykiss). *Sci. Rep.* **2017**, *7*, 46582.

(12) Mauter, M. S.; Palmer, V. R. Expert elicitation of trends in Marcellus oil and gas wastewater management. *J. Environ. Eng.* **2014**, *140* (5), B4014004.

(13) Shaffer, D. L.; Arias Chavez, L. H.; Ben-Sasson, M.; Romero-Vargas Castrilloén, S.; Yip, N. Y.; Elimelech, M. Desalination and reuse of high-salinity shale gas produced water: drivers, technologies, and future directions. *Environ. Sci. Technol.* **2013**, *47* (17), 9569−9583.

(14) Guan, G.; Wang, R.; Wicaksana, F.; Yang, X.; Fane, A. G. Analysis of membrane distillation crystallization system for high salinity brine treatment with zero discharge using Aspen flowsheet simulation. *Ind. Eng. Chem. Res.* **2012**, *51* (41), 13405−13413.

(15) McGinnis, R. L.; Hancock, N. T.; Nowosielski-Slepowron, M. S.; McGurgan, G. D. Pilot demonstration of the NH3/CO2 forward osmosis desalination process on high salinity brines. *Desalination* **2013**, *312*, 67−74.

(16) Li, M. Optimal plant operation of brackish water reverse osmosis (BWRO) desalination. *Desalination* **2012**, *293*, 61−68.

(17) Li, M.; Noh, B. Validation of model-based optimization of brackish water reverse osmosis (BWRO) plant operation. *Desalination* **2012**, *304*, 20−24.

(18) Oke, D.; Majozi, T.; Mukherjee, R.; Sengupta, D.; El-Halwagi, M. Simultaneous Energy and Water Optimisation in Shale Exploration. *Processes* **2018**, *6* (7), 86.

(19) Lopez Diaz, D. C.; Fernando Lira-Barragán, L.; Rubio-Castro, E.; You, F.; Ponce-Ortega, J. Optimal design of water networks for shale gas hydraulic fracturing including economic and environmental criteria. *Clean Technol. Environ. Policy* **2018**, *20* (10), 2311−2332.

(20) Nolte, K. Determination of proppant and fluid schedules from fracturing-pressure decline. *SPE Prod. Eng.* **1986**, *1* (04), 255−265.

(21) Gu, H.; Desroches, J. In New pump schedule generator for hydraulic fracturing treatment design, SPE Latin American and Caribbean petroleum engineering conference; Society of Petroleum Engineers 2003.

(22) Dontsov, E.; Peirce, A. A new technique for proppant schedule design. *Hydraul. Fract. J.* **2014**, *1* (3).

(23) Siddhamshetty, P.; Kwon, J. S. I.; Liu, S.; Valkó, P. P. Feedback control of proppant bank heights during hydraulic fracturing for enhanced productivity in shale formations. *AIChE J.* **2018**, *64* (5), 1638−1650.

(24) Yang, S.; Siddhamshetty, P.; Kwon, J. S.-I. Optimal pumping schedule design to achieve a uniform proppant concentration level in hydraulic fracturing. *Comput. Chem. Eng.* **2017**, *101*, 138−147.

(25) Siddhamshetty, P.; Yang, S.; Kwon, J. S.-I. Modeling of hydraulic fracturing and designing of online pumping schedules to achieve uniform proppant concentration in conventional oil reservoirs. *Comput. Chem. Eng.* **2018**, *114*, 306−317.

(26) Siddhamshetty, P.; Wu, K.; Kwon, J. S.-I. Optimization of simultaneously propagating multiple fractures in hydraulic fracturing to achieve uniform growth using data-based model reduction. *Chem. Eng. Res. Des.* **2018**, *136*, 675−686.

(27) Siddhamshetty, P.; Wu, K.; Kwon, J. S.-I. Modeling and control of proppant distribution of multi-stage hydraulic fracturing in horizontal shale wells. *Ind. Eng. Chem. Res.* **2019**, *58*, 3159.

(28) Singh Sidhu, H.; Siddhamshetty, P.; Kwon, J. Approximate Dynamic Programming Based Control of Proppant Concentration in Hydraulic Fracturing. *Mathematics* **2018**, *6* (8), 132.

(29) Etoughe, P.; Siddhamshetty, P.; Cao, K.; Mukherjee, R.; Kwon, J. S., II Incorporation of sustainability in process control of hydraulic fracturing in unconventional reservoirs. *Chem. Eng. Res. Des.* **2018**, *139*, 62−76.

(30) Elsayed, N. A.; Barrufet, M. A.; El-Halwagi, M. M. Integration of Thermal Membrane Distillation Networks with Processing Facilities. *Ind. Eng. Chem. Res.* **2014**, *53* (13), 5284−5298.

(31) Gregory, K. B.; Vidic, R. D.; Dzombak, D. A. Water management challenges associated with the production of shale gas by hydraulic fracturing. *Elements* **2011**, *7* (3), 181−186.

(32) Lawson, K. W.; Lloyd, D. R. Membrane distillation. *J. Membr. Sci.* **1997**, *124* (1), 1−25.

(33) Oh, H.-J.; Choung, Y.-K.; Lee, S.; Choi, J.-S.; Hwang, T.-M.; Kim, J. H. Scale formation in reverse osmosis desalination: model development. *Desalination* **2009**, *238* (1−3), 333−346.

(34) Liu, S.; Valkó, P. P. Optimization of Spacing and Penetration Ratio for Infinite-Conductivity Fractures in Unconventional Reservoirs: A Section-Based Approach. *Spe Journal* **2017**, *22* (06), 1877−1892.

(35) Hayes, T. *Sampling and Analysis of Water Streams Associated with the Development of Marcellus Shale Gas*; Gas Technology Institute, 2009.

(36) Siddhamshetty, P.; Kwon, J. S.-I. Model-based feedback control of oil production in oil-rim reservoirs under gas coning conditions. *Comput. Chem. Eng.* **2018**, *112*, 112−120.

(37) Rowen, E. L.; Engle, M. A.; Kraemer, T. F.; Schroeder, K. T.; Hammack, R. W.; Doughten, M. W. Geochemical and isotopic evolution of water produced from Middle Devonian Marcellus shale gas wells, Appalachian basin, PennsylvaniaGeochemistry of Produced Water from Marcellus Shale Water, PA. *Aapg Bulletin* **2015**, *99* (2), 181−206.

DOI: 10.1021/acs.iecr.9b01553
Ind. Eng. Chem. Res. 2019, 58, 12097−12115

(38) Misener, R.; Floudas, C. A. ANTIGONE: algorithms for continuous/integer global optimization of nonlinear equations. *Journal of Global Optimization* **2014**, *59* (2−3), 503−526.
(39) Yu, W.; Zhang, T.; Du, S.; Sepehrnoori, K. Numerical study of the effect of uneven proppant distribution between multiple fractures on shale gas well performance. *Fuel* **2015**, *142*, 189−198.
(40) Kondash, A. J.; Albright, E.; Vengosh, A. Quantity of flowback and produced waters from unconventional oil and gas exploration. *Sci. Total Environ.* **2017**, *574*, 314−321.
(41) Kondash, A.; Vengosh, A. Water footprint of hydraulic fracturing. *Environ. Sci. Technol. Lett.* **2015**, *2* (10), 276−280.

DOI: 10.1021/acs.iecr.9b01553
Ind. Eng. Chem. Res. 2019, 58, 12097−12115